Heliyon 10 (2024) e29743

Contents lists available at ScienceDirect

Heliyon

journal homepage: www.cell.com/heliyon

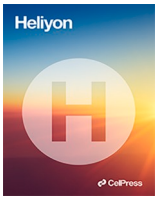

Review article

Electrochemical sensors modified with iron oxide nanoparticles/nanocomposites for voltammetric detection of Pb (II) in water: A review

Joseph Jjagwe [a,*], Peter Wilberforce Olupot [a], Robinah Kulabako [b], Sandro Carrara [c]

[a] *Department of Mechanical Engineering, College of Engineering, Design, Art and Technology, Makerere University, P.O. Box 7062, Kampala, Uganda*

[b] *Department of Civil and Environmental Engineering, College of Engineering, Design, Art and Technology, Makerere University, P.O. Box 7062, Kampala, Uganda*

[c] *Bio/CMOS Interfaces Laboratory, School of Engineering, Institute of Microengineering, École Polytechnique Fédérale de Lausanne (EPFL), Neuchâtel, Switzerland*

ARTICLE INFO

Keywords:
Metal oxide
Voltammetry
Functionalization
Working electrode
Lead
Drinking water

ABSTRACT

Permissible limits of Pb^{2+} in drinking water are being reduced from 10 μgL^{-1} to 5 μgL^{-1}, which calls for rapid, and highly reliable detection techniques. Electrochemical sensors have garnered attention in detection of heavy metal ions in environmental samples due to their ease of operation, low cost, and rapid detection responses. Selectivity, sensitivity and detection capabilities of these sensors, can be enhanced by modifying their working electrodes (WEs) with iron oxide nanoparticles (IONPs) and/or their composites. Therefore, this review is an in-depth analysis of the deployment of IONPs/nanocomposites in modification of electrochemical sensors for detection of Pb^{2+} in drinking water over the past decade. From the analyzed studies (n = 23), the optimal solution pH, deposition potential, and deposition time ranged between 3 and 5.6, −0.7 to −1.4 V vs Ag/AgCl, and 100–400 s, respectively. Majority of the studies employed square wave anodic stripping voltammetry (n = 16), in 0.1 M acetate buffer solution (n = 19) for detection of Pb^{2+}. Limits of detection obtained (2.5 x 10^{-9} - 4.5 μg/L) were below the permissible levels which indicated good sensitivities of the modified electrodes. Despite the great performance of these modified electrodes, the primary source of IONPs has always been commercial iron-based salts in addition to the use of so many materials as modifying agents of these IONPs. This may limit reproducibility and sustainability of the WEs due to lengthy and costly preparation protocols. Steel and/or iron industrial wastes can be alternatively employed in generation of IONPs for modification of electrochemical sensors. Additionally, biomass-based activated carbons enriched with surface functional groups are also used in modification of bare IONPs, and subsequently bare electrodes. However, these two areas still need to be fully explored.

1. Introduction

Lead (Pb) is a non-disintegrative heavy metal present in the Earth's crust, at concentrations of about 0.002 % [1]. Pb is used in

* Corresponding author.
E-mail address: joseph.jjagwe@mak.ac.ug (J. Jjagwe).

https://doi.org/10.1016/j.heliyon.2024.e29743
Received 9 January 2024; Received in revised form 15 April 2024; Accepted 15 April 2024
Available online 16 April 2024

process industries such as metal plating, battery manufacturing, industries engaged in lead–acid batteries, paint, oil, metal, phosphate fertilizers, electronics, and wood production [2]. As such, it is regarded as the most common heavy metal pollutant in the environment [3]. In its ionic state (Pb^{2+}), lead is toxic to humans even at very small concentrations [4,5]. This is due to its ability to induce oxidative stress, and biologically replace other essential metals [6] as well as being an enzyme inhibitor [7]. When absorbed, Pb^{2+} bio-accumulates and is inertly stored in organs such as kidneys, liver and central nervous system [8]. From these organs, it is remobilized leading to chronic health risks such as abdominal pain, high blood pressure, stomach and lung cancers, kidney damage, headache, and nerve damages [5]. On this regard, Pb is considered to be carcinogenic to humans [9]. Moreover, more than half million human deaths per year on a global scale are caused by exposure to Pb [10]. Being neurotoxic, exposure of Pb to children below the age of 7 could cause developmental impairments [11] resulting into poor school performance, decreased IQ, juvenile delinquency, and increased hyperactivity disorder [12].

The maximum allowable concentration of Pb^{2+} in drinking water as set by international and most country-based bodies is 10 μg/L. Nevertheless, a stricter limit of 5 μg/L is proposed by World Health Organization [13]. However, many developing countries fail to meet these limits due to lack of infrastructure for water treatment [8]. In order to mitigate Pb^{2+} pollution and keep water quality up to standards, it is imperative to devise means of early detection of this heavy metal within environmental water bodies. Conventionally, Pb^{2+} is detected using analytical and/or physicochemical techniques such as atomic absorption spectrometry, atomic fluorescence spectrometry, cold vapor atomic fluorescence spectrometry, inductively coupled plasma optical emission spectrometry, inductively coupled plasma-atomic emission spectrometry, inductively coupled plasma mass spectrometry, liquid chromatography, UV–vis spectrometry, capillary electrophoresis, and Laser-Induced Break-down Spectroscopy. Despite the high selectivity, sensitivity, and low detection limits offered by these methods, they are associated with a number of limitations such as; sophisticated sample preparation, costly equipment, lengthy detection times, need of trained personnel, and inability for *in-situ* analysis [14–16]. This thus calls for alternative methods of detecting Pb (II) ions from water samples in a timely low-cost manner without compromising on detection abilities.

Electrochemical sensing is a viable replacement of the conventional detection methods due to advantages such as low detection limits (up to femptomolar), rapidness, low-cost equipment utilized for sensing, real time qualitative and quantitative analyses of complex samples with high sensitivity, short response time, long lifetime (stability) as well as high selectivity relative to interfering components [17,18]. Additionally, electrochemical sensors can be reduced in size (miniaturization) through micro-fabrication methods without affecting their analytical performance [19]. The user-friendliness, and requirement of simple instrumentation enables the integration of electrochemical sensors into automatic fluidic structures for monitoring a wide range of heavy metal ions (HMIs) making them superior to spectroscopic techniques [16]. Moreover, the defined redox potentials of heavy metals permit their direct sensing by electrochemical sensors, and consequently eliminates the demand of a molecular recognition probe that is used in optical sensors [20]. Amongst the available electrochemical techniques, voltammetry is the only method that has high sensitivity for *in-situ* identification, and detection of HMIs pollution [21].

In electrochemical sensors, the character of the working electrode (WE) is very crucial in achieving selectivity, sensitivity, and detection limits of the target analyte [14,22]. However, bare WEs are characterized with limitations such as; low electron transfer rates, passivation of the surface as a result of accumulation of analyte species, sensitivity to temperature fluctuations which may lower their detection ability, high over-potentials and overlapping of peak potentials, as well as low surface area and functional groups [23–25]. Additionally, since environmental samples usually contain a number of pollutants with varying concentrations, the sensitivity and detection limits of electrochemical sensors need to be further improved [18]. Such issues have attracted research into the use of mediators/modified electrodes so as to improve electrochemical responses. The deployed modifier should effectively interact with the target analyte, and facilitate electron transfer so as to achieve increased sensitivity, selectivity, fast response time, good linearity, lower detection limit, stability, and long lifetime [26,27]. Nanomaterials, essentially metal oxide nanoparticles are recently being deployed in electrochemical sensor modifications [28]. This is because the oxides permit good orientation of moieties onto the electrode surface, decrease the distance between electro-active species and the transducer surface, decrease the sensor's working potential, thus fastening the electron transfer rate [29–32].

Iron oxide is the commonest metal oxide used in modification of sensors for detection of pollutants especially heavy metals [33]. The use of iron oxides particularly those of the nanoscale is attributed to their biocompatibility and nontoxicity [34], as well as the high catalytic selectivity of target pollutants [35]. Additionally, sensors based on iron oxide nanostructures are characterized by fast retrieval and response times, room temperature operation, low power consumption, and less ecological degradation [36]. The iron oxide phase, magnetite (Fe_3O_4) which is commonly used in modification of sensors has high magnetic properties which enable it to easily adsorb on the electrode surface [37]. Furthermore, the presence of Fe^{2+} and Fe^{3+} in Fe_3O_4 permits electron hopping process between the two ions, thus increasing the electrical conductivity even at room temperature [33,38]. The Fe–*O*–Pb bond formed between iron oxide and Pb (II) ions ensures good selectivity during electrochemical analysis [39].

Nonetheless, in their operation, bare iron oxide nanoparticles (IONPs) are limited by low specific surface area, agglomerations [40,41], mediator leakages [24], aggregations as a result of structure stacking [27], as well as limited functional groups and porous structure [42]. Moreover, the intrinsic conductivity of iron oxide is poor [43]. Such properties limit pollutant access, and also reduce electro-active area, selective binding sites, and electron transfer during electrochemical processes. These challenges can be addressed by functionalization of IONPs with other reagents. A number of materials including organics, inorganics, and polymers are used to functionalize IONPs for enhanced properties. Moreover, electrochemical sensors modified with iron oxide and other materials such as SiO_2 [44], D-valine [45], guanine [46], NiO [47], Polyamidoamine dendrimer [42], citrate [48], and graphene-bismuth composite [49] have showed higher selectivity with lowest detection limits towards Pb^{2+} in presence of other divalent HMIs at the same concentrations. It is worth mentioning that most of the recent reviews generically discuss the detection of heavy metals in water using various

materials [15,16,33,50–53]. However, there is hardly any review focusing on the use of a specific material for detection of a specific heavy metal ion. Therefore, this review is a comprehensive outlook on the recent developments on the use of iron oxide nanoparticles/nanocomposites for voltammetric detection of Pb^{2+} in drinking water. The choice of the material (s) and pollutant are justified by their unique properties, and detrimental effects to human health, respectively as earlier discussed. The review starts with an overview of electrochemical sensing techniques with emphasis on voltammetry. This is followed by a description of the common methods used to generate IONPs and why functionalization of these bare nanoparticles is key in electrochemical analysis. The performance of working electrodes modified with IONPs/nanocomposites is also discussed as well as the key factors which affect the performance of these modified sensors in detection of Pb^{2+}. Lastly, insights into future research prospects are presented. Aim of this review is then to provide a broader picture on which materials to select as well as the operating conditions for high selectivity, sensitivity, and enhanced detection of Pb^{2+} ions in water.

2. A brief introduction to electrochemical sensors

Electrochemical sensors are devices that convert information obtained from electron transfer between the surface of the sensor and target analyte into readable electrical signals such as current, potential, electrochemical impedance, and electroluminescence [54–56]. The generated signal is proportional to either the concentration of the analyte or its tendency to transfer electrons towards the sensor's surface. The reduction and/or oxidation reactions (redox reactions) of the target analyte is the fundamental phenomenon generating these response signals [57]. Electrochemical measurements are usually carried out in a three–electrode system consisting of a working electrode (WE), a reference electrode (RE) and a counter electrode (CE). All these electrodes are immersed in the same electrolyte. In this system, a reference potential is applied between the WE and RE, whilst current is measured between the WE and CE [33]. Typically, the measured current corresponds to the detection signal. The WE can primarily be a carbon paste electrode (CPE), indium tin oxide (ITO) electrode, glassy carbon electrode (GCE), screen-printed carbon electrode (SPCE), and gold electrode (AuE). The commonest REs used are the saturated calomel electrode (SCE), and the Ag/AgCl electrode. The materials on the WE are required to have high electric conductivity, sensitivity, catalytic activity, with fast response to any changes in analyte concentration [23,34]. Electrochemical sensors are normally operated on the principles of conductometry (due to conductance changes), potentiometry (due to membrane potential changes), impedimetry (due to impedance changes), as well as amperometry and voltammetry (due to changes in current as result of the applied voltage) [16,29,56]. These techniques are schematically shown in Fig. 1 (A, B, C, D, E and F) representing cyclic voltammetry, linear voltammetry, amperometry, impedimetry, potentiometry, and conductometry, respectively. Further discussions of impedimetry and voltammetry are given in the forthcoming subsections. Key performance indicators of electrochemical sensors are described in Table 1.

2.1. Electrochemical impedance spectroscopy

Electrochemical impedance spectroscopy (EIS) is based on perturbation of an equilibrium or steady state electrochemical system through application of a sinusoidal signal (AC current or AC voltage) over a range of frequencies, and then monitoring the resultant sinusoidal response (complex impedance) at the electrolyte/electrode interface [61]. Due to a great deal of data responses, their visual

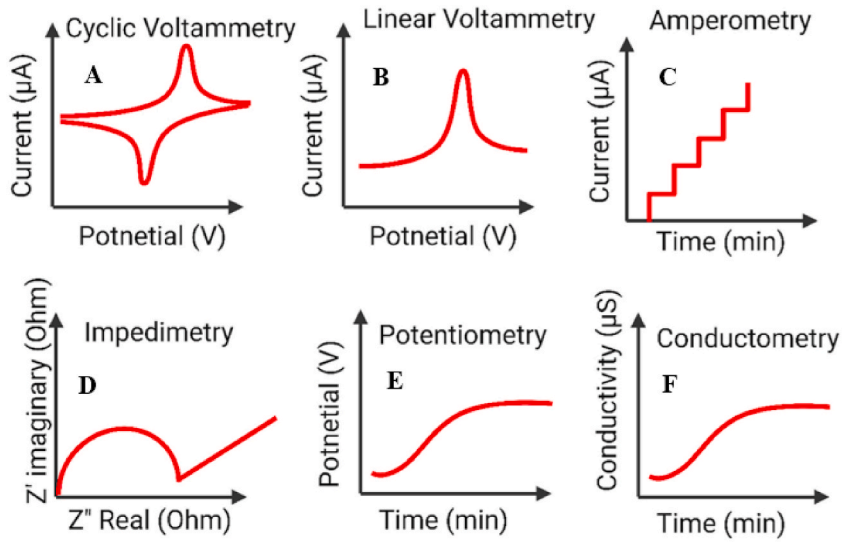

Fig. 1. Schematic diagram of response signals for the commonly used electrochemical techniques in detection of pollutants which include; (A) cyclic voltammetry, (B) linear voltammetry, (C) amperometry, (D) impedimetry, (E) potentiometry, and (F) conductometry [18]: Reproduced with permission from Elsevier B.V under the CC BY license (http://creativecommons.org/licenses/by/4.0/).

Table 1
Performance indicators of electrochemical sensors.

Attribute	Description
Sensitivity	The ratio between a physical parameter and the corresponding output signal [27]. High sensitivity implies that a slightest change in the analyte concentration will result into a noticeable sensor output signal [58,59].
Selectivity	The capability of the sensor to distinguish the response of other competing substances while generating maximum output of the target analyte [19]. In order to ascertain the selectivity of the electrode towards the target ion without any ubiquity, voltammetry experiments are carried out in presence of some of the commonly studied interfering ions. High selectivity of a sensor ensures its extended lifetime, and accuracy [58].
Response time	The time elapsed from the moment the analyte gets into contact with the recognition element to when the signal is received.
Limit of detection (LOD)	This is the lowest concentration (amount) of the analyte that can be reliably quantified. The universal expression for determining LOD is 3(SD/S), where SD = standard deviation of the blank solution and S = slope of the calibration curve.
Reproducibility	The ability of the sensors independently prepared under the same experimental conditions at different times (batches) to generate the same output signal. This, thus depicts the consistency of measurements of the sensor.
Stability	The capability of the sensor to maintain its working performance for a certain period of time. Stability indicates the degree of susceptibility in response to an external disturbance/interference.
Repeatability	The outcome of multiple single tests of a sensor on the same sample under the same conditions [60].

analysis is not plausible, and thus simplification is achieved through modelling the data to a proper equivalent electrical circuit which consists of resistors, capacitors and inductors [16], or constant phase elements [62]. The circuit parameters (e.g, resistance and capacitance) are obtained by fitting the plot of the real and imaginary part of the impedance as described by frequency-trends in Nyquist diagrams/plots [63,64].

The generated Nyquist plots are dependent on the electrochemical mechanism of the equivalent circuit model [65]. The plot typically shows one or more semi-circle portions and sometimes a straight-line region. The semi-circle is obtained at high frequencies and its diameter represents either charge transfer and/or electrode' resistances, with bigger diameters indicating increased resistances [58,65]. It is the charge transfer resistance that is normally used to describe the activity of the electrode towards a given analyte. This resistance depends on insulating features at the electrolyte/electrode interface, while the equivalent capacitance depends on its dielectric features [66]. On the other hand, the straight line portion due to low frequencies is related to diffusion of species onto the electrode [67,68].

The vast application of EIS lies in its ability to provide information regarding interfacial properties/interactions of electrodes [18,69], and to differentiate between the various physical and electrochemical processes within electrochemical systems [62]. Additionally, EIS facilitates the use of direct label free detection, thus making analysis low cost, faster, and easier [65]. In-fact, EIS has been greatly used as the first step to select the best iron oxide based modified working electrode for detection of Pb^{2+} [70–75]. Details accounting for EIS such as developing the equivalent electrical circuits, and their subsequent interpretations have been published elsewhere [61,76,77].

2.2. Voltammetry

Voltammetry is an electrochemical method based on current measurements under scanning bias potential in an electro-active solution [15,16,33]. In this method, controlled time-dependent variable potentials are applied to the WE which is relative to a scanned potential applied to the RE in an electrochemical cell [78]. The resultant current which is generated due to redox reactions of the analyte at the WE, is measured between the WE and CE principle [79]. The redox reaction generates a peak current, called Faradaic current, which is correlated to the analyte's concentration, thus providing specific quantitative analytical information [19]. The current measurements are then plotted against the applied potential to come up with a graph known as a voltammogram. Electrochemical voltammetry is carried out for different reasons such as; studies on redox processes, electron transfer and reaction mechanisms, kinetics of electron transfer processes, thermodynamic properties of species, and adsorption processes on electrode surfaces [57]. Voltammetry is reported as the only electrochemical method with high sensitivity for *in-situ* identification and detection of heavy metal ions (HMIs) pollution [21]. Voltammetric techniques are categorized into potential scan (linear sweep voltammetry and cyclic voltammetry), potential step (normal pulse voltammetry, square wave voltammetry, and differential pulse voltammetry), and stripping voltammetry. All these techniques have advantages of providing qualitative information obtained from the potential location of the peak current as well as quantitative information obtained from the peak current intensity of the redox reaction of the target analyte [19].

2.2.1. Potential scan techniques

Linear sweep voltammetry (LSV) is the simplest voltammetric technique which involves applying a linear potential ramp at a constant scan rate, and measuring the resultant current. LSV is, however, limited by the high detection limits since it can only be used for concentrations higher than 10^{-5} M [79]. Cyclic voltammetry (CV) involves linearly scanning the potential in one direction (forward scan) and then reversing it (reverse scan) at a fixed scan rate to create a cyclic pattern. The resultant current, which is proportional to the electrochemical reaction rate is measured [80]. CV is the commonest technique used to obtain qualitative information about electrochemical reactions. Its capability stems from the rapid insights about the thermodynamics of redox processes, analytes' chemical reactions, and kinetics of heterogeneous electron-transfer events [57]. From the CV voltammogram, peak cathodic potential, E_{Pc} (obtained due to a potential sweep in more negative values, i.e reduction), and peak anodic potential E_{Pa} (obtained due to potential

sweep toward more positive values, i.e oxidation) is obtained. The resultant cathodic (I_{Pc}) and anodic (I_{Pa}) peak currents are also established. Peak current (s) is distinctive to electron transfer and concentration of electro-active species [30] while the difference between E_{Pc} and E_{Pa}, known as the peak to peak separation (Δp) indicates the nature of the redox reaction [81]. Additionally, CV is employed in modification of the WE surface by electrochemical activation or electro-polymerization [22,65]. Like LSV, CV is limited by the high limits of detection within a range of 10^{-3}-10^{-5} M [79].

2.2.2. Potential step techniques

Normal pulse voltammetry (NPV) involves applying discrete potential pulses in an incremental manner with constant time intervals, and measuring the current at the end of each pulse [80]. The resultant voltammograms have a sigmoidal shape. NPV is mainly used when the condition of the electrode surface should be kept constant throughout the entire potential scan [82]. NPV offers higher sensitivity than CV and LSV though with limitations of indistinct signal identification due to high background current [79]. Differential pulse voltammetry (DPV) involves applying incremental constant amplitude potential pulses with time [65]. For each applied pulse, two current measurements (one before, and the other towards the end) are taken, and the difference between these currents is plotted against staircase potential hence generating a voltammogram with a peak-shaped wave form [83]. This technique is associated with high signal-to-noise ratios and rapid decay of charging current thus generating better detection limits and selectivity of target analytes when compared to CV and LSV [15]. DPV has advantages such as; low Limit-Of-Detection (LOD) in the range of $10^{-4} - 10^{-7}$ M, suitable for slow reaction kinetics, suitable for all redox reactions (reversible, quasi-reversible and irreversible), and better sensitivity for multiple analyte systems [79].

Square wave voltammetry (SWV) involves superimposing repetitive square-shaped potential pulses on a staircase potential sweep [15]. The current is measured as a result of the difference between the end of the forward (oxidation), and the end of the reverse (reduction) pulses. These currents are then plotted against the swept potential to obtain a peak-shaped voltammogram, where the peak height correlates to the concentration of the target analtye. SWV is considered the fastest and most sensitive electrochemical technique with the obtained LODs greater than those for chromatographic and spectroscopic analyses [65]. Additionally, SWV requires high frequency inputs resulting into reduced analysis time [58]. Both DPV and SWV are characterized with insignificant capacitive current which leads to enrichment of sensitivity [19,84]. For both techniques, only faradaic currents are measured which results into low disturbances during measurement of low concentrations of analytes [79].

2.2.3. Stripping voltammetry

Stripping voltammetry (SV) is the commonest voltammetric technique used in the detection of target analytes [17]. SV is split into three categories which include: anodic stripping voltammetry (ASV) where analyte stripping is achieved in a more positive potential, cathodic stripping voltammetry (CSV) where analyte stripping occurs in a more negative potential, and adsorptive stripping voltammetry (AdSV) where the analyte is first adsorbed onto the surface of the WE [65]. ASV is the commonly used approach for detection of HMIs, and it comprises of two steps which are; deposition and stripping. The deposition/accumulation/pre-concentration step involves applying a cathodic (negative) potential scan for a given time through magnetic stirring so that the HMIs are reduced and deposited on WE surface [15,85]. The rate of accumulation depends on the WE area, concentration of the analyte, and diffusion properties of the electrolyte solution [15]. According to Lu et al. [21], the accumulation step of HMIs in ASV is achieved by either Faraday's reaction or adsorption. In Faraday's reaction, the HMI is reduced to zero -valent metal under constant negative potential, and then deposited to the WE surface. On the other hand, adsorption involves a reaction between the HMI and the ligands on the WE surface to form complexes which reduce the HMI to its zero-valent state. Following deposition, is the stripping (measurement) step where anodic (positive) potential scan is applied so that the deposited HMI is oxidized and stripped off into ionic form hence generating a faradaic current that is proportional to the concentration of the HMI. ASV offers advantages of low detection limits ($10^{-6} - 10^{-11}$ M), no requirements for water pretreatment, as well as better sensitivity, selectivity and specificity when compared to other voltammetric techniques [50,79]. The specificity of ASV is based on the fact that each metal oxidizes at a specific potential [20]. Additionally, ASV detects the concentration of free HM at the sample pH, unlike many other detection techniques such as spectrometry, which require a strong acidified environment to force all the HMIs into free state [86]. The application of CSV and AdSV in analysis of species has been described in other studies [50,52,79].

Noteworthy, these techniques are combined to increase sensitivity, selectivity, response time and with low limits of detection due to the rapid shrinkage of background noise [45]. Such common combinations include: linear sweep anodic stripping voltammetry (LSASV), differential pulse anodic stripping voltammetry (DPASV) and square wave anodic stripping voltammetry (SWASV). DPASV and SWASV are commonly used for HMIs detection because of their ability to offer simultaneous and individual analysis of target ion(s) [87].

3. Preparation of iron oxide nanoparticles for applications in electrochemical sensors

There are mainly three iron oxide crystalline phases commonly employed in environmental applications. These are magnetite (Fe_3O_4), maghemite (γ-Fe_2O_3), and hematite (α-Fe_2O_3). Both magnetite and maghemite are ferromagnetic with cubic spinel structures while hematite is anti-ferromagneic with a rhombohedral system [88]. The anti-ferromagnetic nature of hematite limits its application in most of the environmental processes [89]. These three phase are n-type semiconductors with a band energy gap of 1.9–2.1 eV [90,91]. The orientation of oxygen and iron ions in the lattice structures of these phases, as well as the associated stabilities in aqueous solutions has been described by Jjagwe et al. [92]. It is important to understand the existing phases since they have an effect on the electrochemical detection of pollutants. For instance, the influence of α-Fe_2O_3 and γ-Fe_2O_3 nanoflowers modified glassy carbon

electrodes on the detection of Pb (II) was studied by Li et al. [93] in the concentration range of 0.1–1.0 nM using SWASV. Their results indicated that γ-Fe_2O_3 exhibited three-fold higher sensitivity than α-Fe_2O_3. This was attributed to the vacant cation sites and many hydroxyl groups on γ-Fe_2O_3 which enhanced the adsorption of Pb^{2+} resulting into higher sensitivity with a lower limit of detection. Noteworthy, vast majority of studies utilized magnetite (Fe_3O_4) and/or it functionalized forms to develop electrochemical sensors for detection of Pb^{2+} [43,45,70] [–] [72,75,94]. This is because magnetite contains both divalent and trivalent iron where Fe^{2+} species occupy octahedral sites, while Fe^{3+} species are equally distributed among both tetrahedral and octahedral sites thus resulting into high crystal field stabilization energy [95]. Additionally, the high saturation magnetization (~92–200 emu/g) of magnetite enables the modified sensors to be easily retrieved from aqueous solution using a permanent magnet [89]. Preparation approaches usually influence the phases of the iron oxide obtained in addition to the resultant morphology, particle distribution and functional groups which in return affect the sensors' performance.

A number of approaches are deployed to generate iron oxide nanoparticles (IONPs). These approaches may be physical (such as ball milling, aerosol, pulsed laser ablation, gas phase deposition, electron beam lithography, and laser induced pyrolysis), biological (such as those mediated by plants, proteins, fungi, and bacteria) or chemical (such as micro-emulsion, co-precipitation, sonochemical, thermal decomposition, electrochemical deposition, hydrothermal). Physical methods are usually incapable of generating nanoscale particles [96], whilst biological approaches are laborious, slow, and associated with low yields [97]. Conversely, chemical methods are tractable, simple, efficient, permit control of shape, size, and compositions [97]. Vast majority of IONPs in literature for electrochemical studies have been prepared by chemical approaches. The three common chemical synthesis methods for preparation of IONPs are co-precipitation, hydrothermal, and sol-gel. These are discussed in the sections that follow. Details about these methods such as the formation mechanisms, associated advantages, and disadvantages have been fully described elsewhere [95,98–100].

Co-precipitation involves mixing ferrous (Fe^{2+}) and ferric (Fe^{3+}) salts in a stoichiometric ratio of1:2 in presence of a base solution at an elevated temperature. The process entails systematic events of nucleation, growth, coarsening, and/or agglomeration with shape and size of the generated IONPs mainly influenced by reaction pH, and temperature [9]. It is desirable to execute the process in an inert (nitrogen) environment especially if Fe_3O_4 is the target phase [101]. Nitrogen prevents oxidation of the iron salts [102]. Without an inert gas, Fe_3O_4 NPs may as well be obtained, provided the reaction time is kept below 1 h to avoid partial oxidation of iron oxides [88]. Co-precipitation yields IONPs with low saturation magnetization and high polydispersity values [103].

Sol-gel is a wet process where monomers are converted into a colloidal solution, called sol, which is then used as a precursor for making the gel that is subsequently heat treated [104]. Four steps are involved in sol-gel approach and these include: (1) hydrolysis and poly-condensation of iron precursor in a solvent to form colloidal suspension of the particles (sol), (2) gelation of the sol to form gel, (3) aging, and (4) drying of the particles through sintering [105]. This method is associated with low temperature and pressure requirements, as well as simple experimental set up [106]. However, it does not favor synthesis of mono-dispersed NPs due to the aggregation effect during washing [100]. Properties of the derived nanoparticles by the sol-gel method are mostly influenced by solution pH, nature of solvent used, type of additives and their concentration, concentration of precursor, pre and post heat treatment of the materials, and aging of the solution [107].

Hydrothermal synthesis utilizes low temperatures (less than 250 °C) and pressures of about 14 MPa to generate metastable nanoproducts [108]. Through this process, experimental parameters such as quantity of modifiers, solution pH, and primary precursors are controlled in a well packed vessel (autoclave) [109]. Water is the key reaction medium for hydrothermal synthesis. If organic solvents such as ethanol, ethylene glycol, and methanol are deployed instead of water, then the process is referred to as solverthermal [110,111]. Hydrothermal synthesis is regarded the most efficient in developing nanoparticles and/or nanocomposites because it favors solubility and crystallization of the reactants due to controlled experimental variables [112]. Besides, the generated products are free of dislocations with better crystallinity than those from other processes [113].

Conventionally, IONPs are derived from a mixture of commercial ferrous and ferric salts in presence of other reagents such as acids, basic solutions and surfactants. However, there are uprising concerns about the cost and environmental sustainability of these conventional approaches. This is due to the involvement of toxic chemicals, and the subsequent unregulated release of harmful by-products in the environment [114,115]. As an alternative to commercial iron-based salts, waste products from steel and iron industries can be used as precursors in synthesizing IONPs. Among the commonly used steel by-products for production of IONPs are mill scale [116–119], steel pickling liquor [120–122], electric arc furnace dust [123,124], iron waste powder [125,126], and others. A detailed review on generation of IONPs from steel wastes for removal of pollutants from water has been presented [92]. However, there is a dearth of information on the utilization of steel waste based iron oxide nanoparticles/nanocomposites for modification of electrochemical sensors.

3.1. *Modification of iron oxide nanoparticles*

As earlier mentioned in section 1, free IONPs have a tendency of agglomeration, leakage, low surface area and limited surface functional groups. Moreover, IONPs are usually unstable and easily gets oxidized in aqueous solutions which limits their dispersibility [127]. Such properties hinder the application in of IONPs in electrochemical sensors due to reductions in: (1) electro-active area, (2) selective binding sites, and (3) electron transfer. Surface modification and/or functionalization of IONPs is a remedy to such limitations. Noteworthy, the electrochemical performance of the modified electrode highly depends on the conductivity and adsorption capacity of the modifier used [128]. Therefore, a desirable modifying agent should contain specific properties which will not only prevent agglomeration but also facilitate pollutant adsorption, hence detection [7]. In electrochemical studies, surface functionalized IONPs play three major roles which include: sample pre-concentration, electrode modification, and as signaling agents [129]. It is advisable to use a mesoporous functionalizing/modifying agent so as to achieve its homogeneous distribution on the surface of IONPs

[130]. A number of materials (organic, inorganic, surfactants, polymers, and ceramics) have been used to modify/functionalize IONPs for enhanced selectivity and sensitivity of Pb (II) as discussed below.

Zhou et al. [131] employed co-precipitation to prepare Fe_3O_4 and Fe_3O_4-chitosan nanocomposite which were later used to modify GCEs for SWASV of Pb^{2+}. Their results indicated that Fe_3O_4-chitosan/GCE showed higher sensitivity (50.6 μA/μM) and lower LOD (0.0422 μM) as compared to 10.5 μA/μM, and 0.140 μM, respectively for Fe_3O_4/GCE. This was attributed to the existence of polar groups (-NH_2, –OH) which provided more adsorptive sites and increased electron transfer on the nanocomposite modified electrode. In another study, Wu et al. [132] compared the sensitivity and LOD of hydrothermally prepared Fe_3O_4/multi-walled carbon nanotubes (Fe_3O_4/MWCNTs) and Fe_3O_4/fluorinated multi-walled carbon nanotubes (Fe_3O_4/F-MWCNTs) towards SWASV of Pb^{2+} in a range of 0.5–30 μM. The results indicated that the fluorinated nanocomposite had higher sensitivity and lower LOD and this was ascribed to strong semi-ionic C–F bonds with strong negative charges that enhanced the adsorption of Pb^{2+} onto the electrode surface.

In order to achieve stability, amplify signals and increase sensitivity of Fe_3O_4 towards Pb^{2+}, a number of modifications were carried out by Nie et al. [71]. Firstly, to increase the chemical stability, silica (SiO_2) was coated onto the surface of Fe_3O_4 through an ultrasonic solvethermal method to form a magnetic core shell of SiO_2@Fe_3O_4. To amplify the electrical signals, gold nanoparticles (AuNPs) were electrostatically adsorbed onto the core shell using 3-aminopropyl-trimethoxysilane as a glue. The amplification was further enhanced by dispersing Au@SiO_2@Fe_3O_4 onto the surface of nitrogen doped graphene (NG) through solvethermal fabrication. Lastly, using an immersion method, L-Cysteine was grafted onto Au@ SiO_2@Fe_3O_4@NG in order to generate carboxyl and amino surface active sites which could easily form Pb^{2+} complexes so as to achieve detection accuracy and rapidity. Elsewhere, Dahaghin et al. [134] also used SiO_2 together with ion-imprinted polymer to functionalize Fe_3O_4, and the generated magnetic nanocomposite was used to modify GCE for detection of Pb^{2+} in water. Silica contains huge amounts of silicon hydroxyl groups (-*Si*-OH) on its surface which improve stability of the nanocomposites, prevent agglomeration of IONPs, and may further bond with other functional groups hence improving the selectivity of target analytes [129,135]. Additionally, the silica core also increases hydrophilicity and biocompatibility of pristine IONPs in addition to offering extra protection against oxidation and aggregation [99].

Pu et al. [75] hydrothermally employed graphitic carbon nitride (g-C_3N_4) and bismuth oxide (Bi_2O_3) to respectively increase adsorption and amalgamation effects of Fe_3O_4/C_3N_4/Bi_2O_3 modified GCE towards Pb^{2+} detection. Elsewhere, Fall et al. [136] developed a rGO@CNT@Fe_2O_3/Ppy composite through hydrothermal reaction and electrodeposition to modify an electrochemical sensor for Pb^{2+}. In this composite, reduced graphene oxide and carbon nanotubes (rGO@CNT) were used to provide more active surface sites and easy electron transfer, while amino functional groups contained in polypyrrole (Ppy) provided a chelating effect towards Pb^{2+}. To achieve increased chelation of Pb^{2+}, for its enhanced selectivity and sensitivity, Dahaghin et al. [134] functionalized rGO@Fe_3O_4 with benzothiazole-2-carboxaldehyde (2-CNT) to come up with a novel rGO@Fe_3O_4@2-CNT modified GCE which achieved a LOD of 0.02 ng/mL for Pb^{2+} in water. RGO is often used to functionalize IONPs due to its characteristics such as large specific surface area, high thermal and electrical conductivities, oxygen-containing surface groups, rapid electron transfer rates, and high tensile mechanical strength that actively improve electrochemical processes [38,68,137]. Bakhsh et al. [138] attributed the superior sensitivity of ZnO/Fe_2O_3/GCE towards Pb^{2+} to the increased oxygen vacancies which acted as electron donors, and thus enhanced the adsorption of the metal ion onto the modified electrode surface. In a related study, the rapid selectivity of Pb^{2+} by Fe_2O_3NP/ZnO--nanorods/indium tin oxide electrode was ascribed to the presence of hydroxyl functional groups which provided electron pairs that led to strong formation of covalent binding with the metal ion [3]. Capping Fe_3O_4 with citrate introduced negative surface charges which enhanced adsorption of Pb^{2+}, and subsequently its rapid detection using citrate@Fe_3O_4/GCE [48]. There are also a number of studies employing different materials for enhancement of IONPs towards detection of Pb^{2+} in water as it will be illustrated in the forthcoming sections. It has been observed that in most cases, the nanocomposite modifier comprises of a number of components which need lengthy preparation procedures and many support reagents. This usually arises challenges of reproducibility and sustainability of the generated electrodes. It is thus important to explore materials with superior properties in terms of functional groups, surface area, conductivity, and stability which may be used as single modification agents for bare IONPs, and hence for existing WEs.

3.2. Characterization of the developed iron oxide nanoparticles/nanocomposites

The performance of the working electrode in electrochemical analysis of pollutants largely depends on the properties of the modifying agent(s) used. Such properties include: particle size, surface charge, surface functional groups, shape, degree of crystallinity, specific surface area, elemental composition, morphology, oxidation state, thermal stability, magnetic characteristics, among other factors. For instance, the effect of morphology (adsorptive sites) and specific surface area (SSA) on detection of Pb (II) was studied by Li et al. [139] through modifying GCE with either α-Fe_2O_3 nanorods (SSA = 108.6 m^2/g) or α-Fe_2O_3 hollow nanocubes (SSA = 150.1 m^2/g). Their observations were as follows; (1) a response signal with hollow nanocubes was observed on addition of 0.7 μM of Pb(II) while for the nanorods, it was at 0.01 μM, (2) the sensitivity of hollow nanocubes was 17.68 μA/μM as compared to the 109.67 μA/μM for the nanorods, (3) the limit of detection (LOD) for the nanocubes was 0.083 μM compared to 0.0034 μM for the nanorods. Furthermore, the amount of Pb (II) adsorbed on nanorods was twice that on the nanocubes with a lower binding energy as observed from XPS analysis. It was thus concluded that adsorptive sites had more influence in detection of Pb (II) than SSA for iron oxide-based sensors. In another study, Liu et al. [43] used a solverthermal process to prepare different Fe_3O_4@mesoporous carbon nano-composites, namely; Fe_3O_4@MPC-1, Fe_3O_4@MPC-2, Fe_3O_4@MPC-3, Fe_3O_4@MPC-4 by varying the volume (0.5, 1.0, 1.5, 2 mL) of 37 % ammonium hydroxide concentration (NH_4OH), respectively. These composites were later used to modify GCEs for detection of Pb^{2+} in water. Their results indicated that increase in the volume of NH_4OH resulted into increased specific surface area in the order of 238.4 > 174.2 > 113.9 > 75.7 m^2/g for Fe_3O_4@MPC-1, Fe_3O_4@MPC-2, Fe_3O_4@MPC-3, and Fe_3O_4@MPC-4, respectively. However, at the same operating conditions, in the linear range of 0.2–50 μM of Pb^{2+}, the obtained LODs were 12.1, 26.7, 31.4, and 34.2 nM for

Fe_3O_4@MPC-2, Fe_3O_4@MPC-3, Fe_3O_4@MPC-4, and Fe_3O_4@MPC-1, respectively. It was thus concluded that a higher specific surface area did not necessary translate into the lowest LOD. The highest sensitivity and lowest LOD of Fe_3O_4@MPC-2 was ascribed to its well distributed mesoporous nanochain structure which favored the adsorption of Pb^{2+} ions.

This background thus justifies why it is important to perform thorough characterization of the developed IONPs and/or

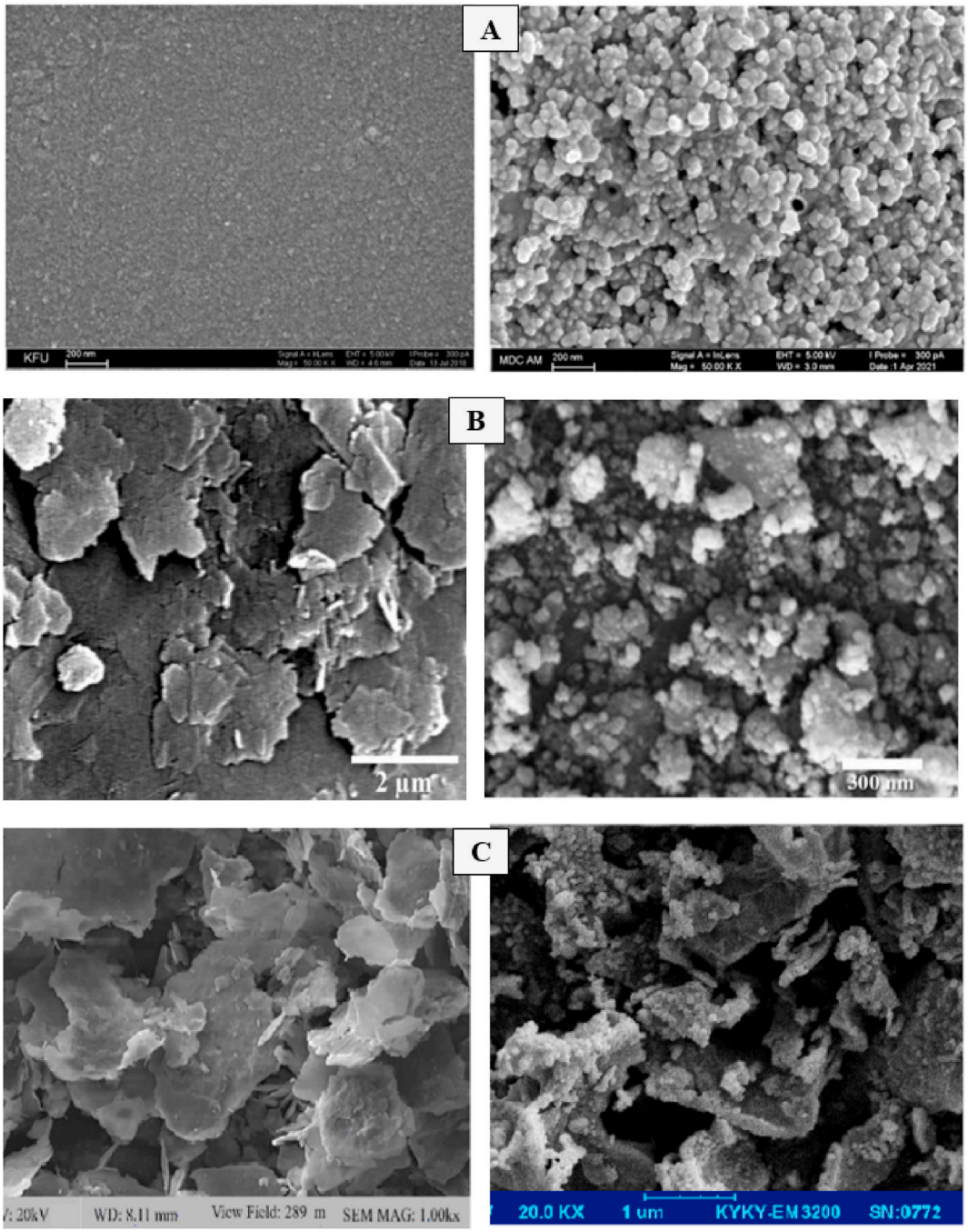

Fig. 2. SEM images showing the surface morphology of: (A) a bare glassy carbon electrode (GCE) on the left, and GCE modified with CeO_2/Fe_2O_3 nanocomposite on the right [141]. Reproduced with permission from MDPI, Copyright (2021) under the terms and conditions of the Creative Commons Attribution (CC BY) license (https://creativecommons.org/licenses/by/4.0/); (B) a carbon paste electrode (CPE) on the left, and a CPE modified with Nitro Benzoil Diphenyl Methylene Phosphorane/Fe_3O_4/ionic liquid (N-BDMP/Fe_3O_4/IL) composite on the right [142]. Reproduced with permission from Iranian Chemical Society, Copyright (2019) under CC BY license (https://creativecommons.org/licenses/by/4.0); (C) a CPE on the left, and a CPE modified with IONPs on the right [143]. Reproduced with permission from Elsevier, Copyright (2020), License number-5673170626380.

nanocomposites before being used as modifiers of working electrodes. A number of techniques exit for characterization of IONPs and its derived nanocomposites. These techniques have been fully described by Jjagwe et al. [92]. Briefly, shape, size, heterogeneity as well as the degree of dispersion and aggregation are shown using Scanning Electron Microscopy (SEM) and/or Transmission Electron Microscopy (TEM) with SEM being the commonly used due to its simplicity in operation [104]. Morphology is a very key parameter since it affects both the surface area and the number of adsorption sites on the surface of nanomaterials [140]. SEM images of some of the electrodes modified with IONPs based materials are shown in Fig. 2 (A-C). It can be seen that, in terms of surface roughness and porosity, the morphology of the modified electrodes is very much distinct from the bare electrodes. This extra surface composition could be responsible for the enhanced adsorption, and thus detection of pollutants during electrochemical studies by modified electrodes. Additionally, SEM can be combined with the Energy Dispersive X-ray (EDX) technique to indicate the elements composing the samples. Surface functional groups are established by Fourier Transform Infrared Spectroscopy (FTIR). Functionalization/modification of bare IONPs is associated with introduction of more functional groups as seen in Fig. 3 (A-D) and this is helpful in increasing the adsorption capacity.

The specific surface area, pore volume, and pore size are commonly obtained using the Brunauer-Emmett-Teller (BET) method through the analysis of adsorption isotherms of nitrogen or some other gas [147]. The crystalline structure issues of the developed materials such as defects, stresses, average grain sizes are established by X-ray Diffractometer (XRD). From XRD peaks, different planes of IONPs are established [115] as well as the degree of interaction of different components during the formation of nanocomposites [148]. Noteworthy, the diffraction peaks of γ-Fe_2O_3 and Fe_3O_4 are quite similar due to the same spinel structure, hence cannot easily be distinguished by only XRD. For this reason, X-ray photoelectron spectroscopy (XPS) analysis supplements XRD for clarification of IONP phases [149]. For indicating the thermal stability and/or capping structure of the functional groups of IONPs, a thermal gravimetric analyzer together with a Differential scanning calorimetry (TGA-DSC) are used. A key feature for the immense deployment of IONPs in environmental applications is their magnetic properties which indicate the possibility of separation and recovery after use. These magnetic properties are commonly determined with a vibrating sample magnetometer (VSM).

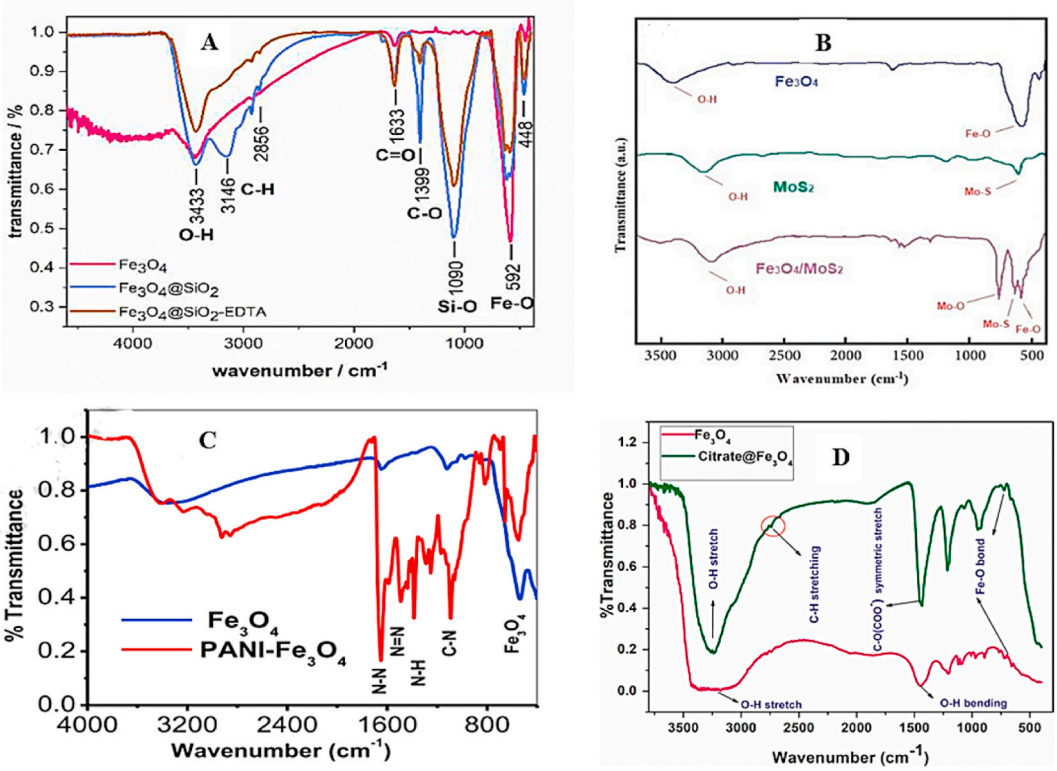

Fig. 3. FT-IR spectra of: (A) Magnetite (Fe_3O_4), Fe_3O_4 functionalized with silica (Fe_3O_4@SiO_2), and Fe_3O_4@SiO_2 functionalized with Ethylenediaminetetraacetic acid (Fe_3O_4@SiO_2-EDTA) [144]. Reproduced with permission from Wiley-VCH, Copyright (2019) under the CC BY license (https://creativecommons.org/licenses/by/4.0); (B) Fe_3O_4, molybdenum disulfide nanosheets (MoS_2), and Fe_3O_4 functionalized with MoS_2 [145]. Reproduced with permission from Elsevier, Copyright (2021), License number- 5673410155217; (C), Fe_3O_4, and Fe_3O_4 functionalized with polyaniline (Fe_3O_4 –PANI) [146]; (D) Fe_3O_4, and Fe_3O_4 functionalized with citrate [48]. Reproduced with permission from Elsevier, Copyright (2021), License number-5673410877692.

4. Modification of working electrodes

There are various methods used to modify surfaces of working electrodes. These include: drop casting, spin coating, dip coating, electro-deposition, paste mixing, screen printing, ink-jet printing, electro-polymerization, and electrophoretic. The fabrication choice depends on the electrode type, the nature of modifier, analytical requirements, and economical possibilities [150]. The two commonly applied techniques for modifying working electrodes with IONPs/nanocomposites are drop-casting, and electrodeposition with the former being the most prominent. In drop-casting, a liquid droplet containing the nanomaterial of interest is deposited on the surface of

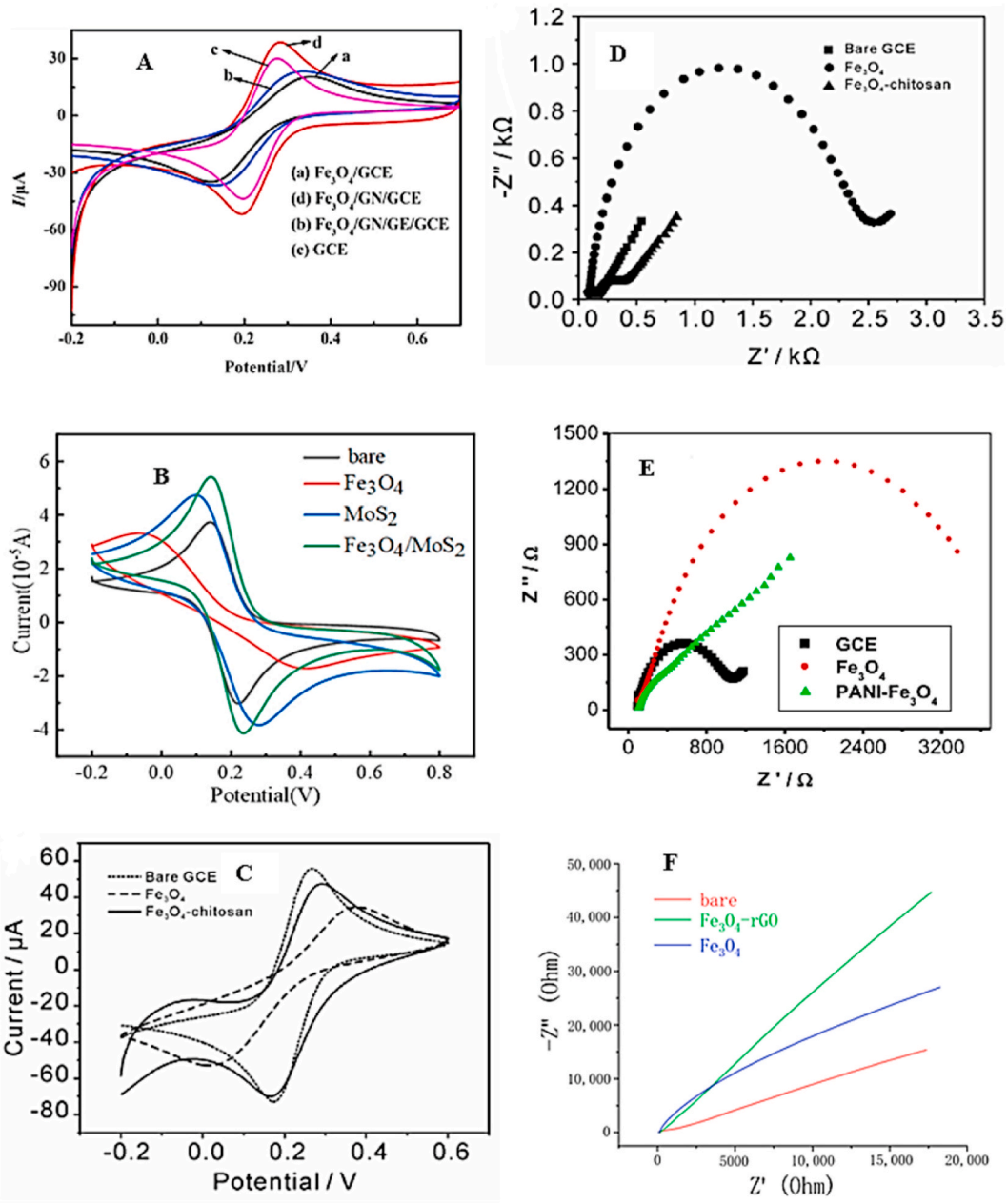

Fig. 4. On the left are cyclic voltammograms, and on the right are EIS Nyquist plots of bare electrodes, and when these electrodes are modified with Fe_3O_4 or its composites. In (A) GN is graphene and GE is garlic extract [74], reproduced with permission from Springer Nature, Copyright (2018). In (B) MoS_2 is Molybdenum disulfide [67] reproduced with permission from MDPI, Copyright (2023) under the CC BY license (https://creativecommons.org/licenses/by/4.0). In (C) and (D), chitosan was used as a modifier for Fe_3O_4 [131], reproduced with permission from Elsevier, Copyright (2016), License number-, 5673770085135. In (E) PANI is polyaniline [146], reproduced with permission from Elsevier, Copyright (2018), License number- 5673780007452. In (F) rGo is reduced graphene oxide [163], reproduced with permission from MDPI, Copyright (2021) under the CC BY license (https://creativecommons.org/licenses/by/4.0). All experiments were carried out in 5 mM $[Fe(CN)_6]^{3-/4-}$ in 0.1 M KCl.

the electrode to be modified. The deposition should be confined to the conductive part of the electrode without spilling over into the insulating surrounding [81]. The solvent used to disperse the nanomaterials have an influence on performance of the modified electrode. For instance, the influence of dimethylformamide (DMF), water, and ethanol in dispersing Fe_3O_4/rGO for modifying glassy carbon electrode (GCE) was studied by Thu et al. [151]. Their results indicated that ethanol displayed 2.2, and 1.2 higher anodic peak currents than DMF, and water, respectively, and was thus selected as the most appropriate dispersant. Prior to the modifications, surfaces of working electrodes are cleaned by either; (1) polishing with alumina (Al_2O_3) or diamond slurries [152] to generate mirror-like surfaces, followed by ultra-sonic washing in ethanol and water under free air or nitrogen [153] or (2) electrochemically cleaning with a known concentration of an acid within a specified voltage range until constant voltammograms are obtained [30]. The polished surface is considered clean if the peak potential difference is below 100 mV [67]. Any adsorbed species left onto the electrode after polishing is removed by also performing several CV scans across a wide potential window until no current peaks are observed [81]. The thickness of the formed film largely depends on the concentration of the modifier [79]. Drop-casting is easy and quick to implement, relatively cheap, and generates relatively thick films [150]. However, the non-uniformity of the cast layer on the surface of the electrode during drop-casting limits the reproducibility of this method [18]. Additionally, the drop cast IONP layer is susceptible to peel off after electrochemical analysis or repeated washings owing to the weak adhesion of IONPs onto the WEs, and this limits stability [154].

In electrodeposition, a potential is applied so that a thin layer of the modifying agent (which is a metal, or an oxide, or an alloy, or salt solution) is deposited on the surface of the electrode immersed inside an electrolyte [79]. Mazloum-Ardakani et al. [155] electrodeposited Fe_2O_3 on a polished GCE by applying a potential sweep from −0.5 to 0.8 V at scan rate of 100 mV/s for 10 cycles in presence of sodium fluoride and hydrogen peroxide. Eeu et al. [156] electrodeposited a nanocomposite layer of polypyrrole/rGO/Fe_2O_3 onto ITO electrode at a fixed potential of +0.8 V (vs SCE) for detection of Pb^{2+} in water. Electrodeposition requires three basic elements which include: (1) an electrochemical bath containing the species to be deposited plus other additives, (2) electrodes, and (3) a system which provides the potential or current difference [78]. The main parameters influencing electrodeposition process are: solution pH, deposition potential, current density, type of working electrode, synthesis time, bath composition, electrolyte, temperature, and impurities/additives present in the solution [18]. All these factors have an effect on the shape, morphology, and size of the electrodeposited material [157,158]. For instance, the effect of deposition potential (−1.15, −1.20, −1.25, and −1.30 V) on the shape, size and magnetic properties of iron oxide film deposited onto a copper electrode was studied by Elrouby et al. [159] using a deposition bath containing 0.12 M Fe^{3+} and 0.2 M triethanolamine in presence of 2 M sodium hydroxide (at a pH of 13.5) at a temperature of 50 °C. Their results indicated that particle size (4–19 nm) and saturation magnetization (214–283 emu/g)

Table 2
Electrochemical properties as determined by CV and EIS for working electrodes modified with iron oxide nanoparticles/nanocomposites.

Working electrode	Modifier used	Redox probe used	Peak to peak separation (ΔE_p, mV)		Peak anodic current (I_{pa}, μA)		Charge transfer resistance (R_{ct}, Ω)		Electrode surface area (cm^2)		Reference
			BE	ME	BE	ME	BE	ME	BE	ME	
GCE	α-Fe_2O_3/MWCNT	2.5 mM $[Fe(CN)_6]^{3-/4-}$ in 0.1 M KCl	100	72	4.39	4.78	222.2	0.001	0.0324	0.040	[165]
GCE	rGO@CNT@Fe_2O_3/Ppy	5 mM $[Fe(CN)_6]^{3-/4-}$ in 0.1 M KCl	134	107	10/cm^2	25/cm^2	140	52.36	0.046	0.078	[136]
GCE	Fe_2O_3	5 mM $[Fe(CN)_6]^{3-/4-}$ in 0.1 M KCl	358	304	106	112	110	43	0.039	0.049	[162]
	Fe_2O_3-GS			104		248		5		0.188	
GCE	Fe_3O_4/MWCNTs/LSG/CS	5 mM $[Fe(CN)_6]^{3-/4-}$ in 0.1 M KCl	221	104	35.79	79.90	462	95	0.0180	0.0676	[166]
CPE	Fe_2O_3	5 mM $[Fe(CN)_6]^{3-/4-}$ in 0.1 M KCl	309	136	15	50			0.116	0.1788	[64]
GCE	Fe_3O_4@CMs	5 mM $[Fe(CN)_6]^{3-/4-}$ in 0.1 M KCl	160	170	30	39	–	–	–	0.032	[72]
	NH_2– Fe_3O_4@CMs			20		55				0.040	
GCE	α-Fe_2O_3	5 mM $[Fe(CN)_6]^{3-/4-}$ in 0.1 M KCl	94	287	39.13	19.35			0.113	–	[167]
GCE	rGO/Fe_3O_4	5 mM $[Fe(CN)_6]^{3-/4-}$ in 0.1 M KCl	450	220	30.2	52.08	100	74	–	–	[66]
GCE	Titanium carbide-α-Fe_2O_3	5 mM $[Fe(CN)_6]^{3-/4-}$ in 0.1 M KCl	94	90	39.13	40.19			0.113	0.18	[167]
GCE	α- Fe_2O_3	5 mM $[Fe(CN)_6]^{3-/4-}$ in 0.1 M KCl					46	312	0.076	0.066	[93]
GCE	γ-Fe_2O_3	5 mM $[Fe(CN)_6]^{3-/4-}$ in 0.1 M KCl					46	225	0.076	0.07	[93]
GCE	Fe_3O_4	2 mM $[Fe(CN)_6]^{3-/4-}$ in 0.1 M KCl	94	89	17	22	210	160	–	–	[161]
	rGO- Fe_3O_4			65		29		75			

Abbreviations: GCE-glassy carbon electrode, CPE-carbon paste electrode, MWCNT-multi-walled carbon nanotubes, CNT-carbon nanotubes, rGO-reduced graphene oxide, LSG-laser scribed graphene, CS-chitosan, GS-graphene sheets, CMs-carbon microspheres, Ppy-polypyrrole. BE-bare electrode, ME-modified electrode.

increased with increase in the applied negative potential. Elsewhere, Nor et al. [154] electrochemically deposited Fe_3O_4–COOH onto an aminopropylitriethoxysilane functionalized ITO (APTES-ITO) electrode by varying the soaking time (30, 60, 90, and 120 min), and observing the effective electrode surface area as well as the peak currents. Their results indicated that the electrode surface areas increased with soaking time which further translated into increased peak anodic currents with highest values of 0.957 cm^2, and 770.02 μA for area and current, respectively obtained at 90 min. However, at a soaking time of 120 min, the electrode surface area (0.704 cm^2), and peak current (566.6 μA) were the least. This was attributed to excess Fe_3O_4–COOH being attracted towards protonated amino groups ($^+NH_3$) of the APTES-ITO electrode, thereby causing agglomeration of the magnetic nanocomposite and thus reducing active surface area available for the redox reaction. Compared to drop-casting, electrodeposition provides more precise control over film thickness and uniformity, though with a more complicated setup and material handling procedure [150].

5. Performance of iron oxide based modified electrodes

The electrochemical behavior of modified electrodes in comparison to bare/pristine electrodes is established by CV and EIS studies using an electrolyte of a given concentration. Ferrocyanide is the often used redox probe to observe the charge transfer kinetics due to its sensitive surface such that even small changes in the surface chemistry of an electrode are identified [3]. The key parameters used to compare the electrode performance are: peak currents, peak to peak separation, charge transfer resistance, and electrode surface area. Usually, the most suitable electrode for voltammetric detection of metal ions is that with the highest peak current and electrode surface area as well as the lowest peak to peak separation and charge transfer resistance. However, it has been observed that modification of WEs with bare IONPs results into reduced peak currents, increased charge transfer resistance (as observed from the increased semi-circle diameter of the Nyquist plot), increased peak to peak separation as well as reduced electrode surface area (Fig. 4 and Table 2). This was attributed to the non-conductivity nature of IONPs which led to increased resistance to electron transfer thus the reduced parameters. Moreover, Fe_3O_4 NPs behave both as capacitors and resistors due to their polarizing and semi-conducting nature, and this characteristic contributes to high electron transfer resistance [160]. Nonetheless, there are studies where IONP modified electrodes display better characteristics than bare electrodes [64,161,162]. The performance of IONP based electrodes is usually improved when nanocomposites are used. Some CV and EIS Nyquist plots of bare electrodes, IONPs, and IONP nanocomposite modified electrodes are shown in Fig. 4 (A-F).

Caution should be taken when selecting the material to be used in functionalizing IONPs. For instance SiO_2@Fe_3O_4/GCE showed a weaker peak current signal when compared to Fe_3O_4/GCE, and this was attributed to the weak conductivity of SiO_2 [71]. Electrodepositing polypyrole (Ppy) onto rGO@CNT@Fe_2O_3 resulted into an increased peak to peak separation attributable to poor reversibility of Ppy doping/undoping processes [136]. Sometimes, higher peak currents and low charge transfer resistances during preliminary selection of the suitable electrode may not necessarily translate into good sensitivity and selectivity of the target pollutant. For example, despite the higher peak to peak separation and charger transfer resistance of Fe_3O_4/GCE electrode, it showed higher sensitivity, selectivity, and lower LOD towards Pb (II) when compared to bare electrodes [164]. The electrochemical characteristics of working electrodes modified with iron oxide-based nanomaterials is shown in Table 2.

5.1. Factors affecting the performance of the modified electrodes

5.1.1. Supporting electrolyte

During the transfer of electrons from the electrode to the analyte, a salt, known as the supporting electrolyte is dissolved in the solvent (which contains the analyte) to decrease the solution resistance to charge transfer. As electron transfer occurs at the electrodes, the supporting electrolyte migrates to balance the charge and complete the electrical circuit, thus this electrolyte should be: (1) highly soluble in the solvent, (2) chemically and electrochemically inert in the conditions of the experiment, and (3) easy to purify [81]. Buffer solutions are widely employed as supporting electrolytes due to their possibility to prevent large pH deviations [168]. Maleki et al. [42] evaluated the effect of 0.1 M buffer solutions of NaAc-Hac, Na_2HPO_4– NaH_2PO_4, and NH_4Cl–HCl, at pH = 5.5 on detection of Pb^{2+} in water using a CPE modified with second generation polyamidoamine dendrimer functionalized magnetic nanoparticles (Fe_3O_4@G2-PAD/CPE). Their results indicated that no signal was found in NH_4Cl–HCl, small peak signal was observed for the Na_2HPO_4– NaH_2PO_4 while a well-defined highest peak current signal was obtained in NaAc-Hac buffer solution. Xiong et al. [161] used rGO-Fe_3O_4/GCE to select the most suitable electrolyte among NaAc-Hac, NH_4Cl–HCl, and phosphate buffer solution (PBS) for voltammetric determination of Pb^{2+} in water. At the same concentration (0.1 M) their results indicated that the highest and most stable current peaks were obtained from NaAc-Hac with two unstable short current peaks observed from PBS, and no peaks were displayed from NH_4Cl–HCl. Similarly, Bai et al. [72] observed strongest and sharpest peak currents with 0.1 M of NaAc-Hac as compared to PBS and NH_4Cl–$NH_3.H_2O$ at the same concentrations when using NH_2–Fe_3O_4@carbon microsphere/GCE. In another study, Wang et al. [169] studied the influence of 1 M of Hac, HCl, H_2SO_4, HNO_3, and H_3PO_4, towards the detection of Pb^{2+} using Fe_3O_4@PDA@M-nO_2/GCE. Their observation indicated no current peaks with Hac, and H_3PO_4, very small peaks with HNO_3, and H_2SO_4, whereas well defined peaks were obtained with HCl. This was analogous to Mohammadi et al. [59] who indicated that well defined DPASV current peaks for detection of Pb^{2+} in water were observed with HCl as compared to $HClO_4$,H_2SO_4, and HNO_3 (at 0.4 M concentration for all electrolytes) using Fe_3O_4/eggshell/multi-walled carbon nanotube/CPE electrode.

The concentration of the support electrolyte has an effect on the sensing abilities of the electrode. According to Elgrishi et al. [81], the use of high concentration of electrolytes is beneficial to increase solution conductivity and limit analyte migration. On the contrary, Moutcine et al. [69] elucidates that high electrolyte concentration may limit electrostatic repulsions and increase particle accumulation resulting into insufficient sites on the electrode surface, and hence a decrease in detection ability of HMIs. Moreover, there is a

Table 3
Performance of electrochemical sensors modified with iron oxide nanoparticles/nanocomposites towards the voltammetric detection of Pb (II) in water.

Iron oxide based working electrode	Electrolyte used	Detection method	Optimal conditions	Concentration range	Sensitivity	Limit of detection	Limit of quantification	Reference
NH_2–Fe_3O_4@carbon microsphere/GCE	0.1 M ABS	SWASV	pH = 5.0, deposition potential = −0.7 V vs Ag/AgCl, deposition time = 150 s	1.0–10.0 μM	1.42 μA/μM	28.5 nM (0.0059 μg/L)	–	[72]
Fe_3O_4@PDA@MnO_2/GCE	1 M HCl	DPV	pH = 3, Modifier volume = 0.1 mg, pre-concentration time = 8 min	0.1–150 μg/L		0.03 μg/L		[169]
Fe_3O_4/D-valine/GCE	0.1 M ABS	SWASV	pH = 5.2, deposition potential = −1.1 V vs SCE, deposition time = 300 s	0.08–2 μM	1.275 μA/nMcm^2	4.59 nM (0.0095 μg/L)		[45]
rGO@CNT@Fe_2O_3/PPy/GCE	0.1 M ABS	SWASV	pH = 4.5, deposition potential = −1.3 V vs Ag/AgCl, deposition time = 300 s	0.02–0.26 μM	162.8 μA/μM	0.1 nM (0.0002 μg/L)	–	[136]
α-Fe_2O_3/NiO/GCE	0.1 M ABS	SWASV	pH = 4.5, deposition potential = −1.1V vs Ag/AgCl, deposition time = 150 s	0.05–0.9 μM	59.8 μA/μM	0.02 μM (0.0414 μg/L)		[47]
α-Fe_2O_3/BCN/Nafion/GCE	0.1 M ABS	DPASV	pH = 4, deposition potential = −1.2 V vs Ag/AgCl, deposition time = 400 s Modifier volume = 2 mg/mL	0.5–140 μg/L	–	0.129 μg/L	–	[39]
Fe_3O_4/Bi_2O_3/C_3N_4/GCE	0.1 M ABS	SWASV	pH = 4.5 deposition potential = −1.1V vs SCE, deposition time = 300 s Modifier volume = 2 mg/mL	0.01–3 μM	–	0.001 μM (0.0021 μg/L)		[75]
Fe_2O_3/ZnONRs/ITOE	0.1 M ABS	SWASV	pH = 5, deposition potential = −1.1 V vs Ag/AgCl, deposition time = 120 s	0.2–3.5 μM	4.40 μA/μM	0.01 μM (0.021 μg/L)		[3]
ae-Fe/Fe_2O_3@CCE	0.1 M ABS	DPASV	pH = 4.5, deposition potential = −1.1 V vs Ag/AgCl, deposition time = 160 s	0.05–2.4 μM	408.8 μA/mM cm^2	0.0015 μM (0.0031 μg/L)	–	[40]
Fe_3O_4@SiO_2@IIP@GCE	0.1 M ABS	DPASV	pH = 5.6, deposition potential = −1.2 V vs Ag/AgCl, deposition time = 360 s	0.1–80 ng/mL	455.7 μA/μM	0.05 ng/mL (0.05 μg/L)	0. 16 ng/mL (0.16 μg/L)	[133]
Fe_3O_4/graphene/garlic extract/GCE	0.1 M ABS	SWV	pH = 5.5, deposition potential = −1.0 V vs Ag/AgCl, deposition time = 180 s Modifier volume = 5 μL	0.001–1000 nM	–	0.0123 pM (2.5 x10^{-9} μg/L)	0.041 pM (8.5 x10^{-9} μg/L)	[74]
Fe_3O_4@polyanilie@nafion@GCE	0.1 ABS	SWASV	pH = 4, deposition deposition time = 180 s Modifier volume = 0.1 mg/mL	0.1–10,000 nM	–	0.03 nM (6.2 x10^{-6} μg/L)	0.09 nM 1.86 x 10^{-5} μg/L)	[37]
Fe_3O_4/eggshell/MWCNTs/CPE	0.4 M HCl	DPASV	pH = 5.5, deposition potential = −1.0 V vs Ag/AgCl, deposition time = 500 s Modifier volume = 5 % (w/w)	0.5–200 ng/mL	–	0.15 ng/mL (0.15 μg/L)	–	[170]
Fe_3O_4/MWCNTs/LSG/CS/GCE	0.1 M PBS	SWASV	pH = 5, deposition potential = −1.2 V vs Ag/AgCl, deposition time = 150 s	1–200 μg/L	–	0.7 μg/L	–	[166]
Fe_3O_4/G2@PAD/CPE	0.1 M ABS	SWASV	pH = 5.5, deposition potential = −1.1 V vs Ag/AgCl, deposition time = 140 s Modifier volume = 20 μL	0.5–80 ng/mL	–	0.17 ng/mL (0.17 μg/L)	–	[42]
Fe_3O_4/GCE	0.1 M ABS	SWASV	pH = 5, deposition potential = −0.9 V vs Ag/AgCl, deposition time = 120 s	0.3–0.8 μM	22.2 μA/μM	0.0699 μM (0.0148 μg/L)		[164]
FePc/SiO_2–Fe_3O_4/GCE	0.1 M PBS	DPSAV	pH = 5.5 deposition potential = −1.0 V vs Ag/AgCl, deposition time = 100 s	10–100 μg/L	0.22 μA/μg/L	4.540 μg/L	–	[152]
Nanorod Fe_2O_3/GCE	0.1 M ABS	SWASV	pH = 5, deposition potential = −1.1 V vs Ag/AgCl, deposition time = 120 s Modifier volume = 5 μL	0.01–0.15 μM	109.67 μA/μM	0.0034 μM (0.0007 μg/L)		[139]
Fe_3O_4/carbon core shell/GCE	0.1 M ABS	SWASV	pH = 5, deposition potential = 0 V vs Ag/AgCl, deposition time = 180 s	0.1–18 μM	95.6 μA/μM	0.17 μM (0.0352 μg/L)	–	[94]
L-cysteine@Au/@SiO_2@Fe_3O_4@NG/GCE)	0.1 M ABS	SWV	pH = 5, deposition time = 100 s, Modifier volume = 8 μL	5–80 μg/L	–	0.6 μg/L		[71]
Fe_2O_3/Graphene/Bismuth/GCE	0.1 M ABS	DPASV	pH = 4.5, deposition potential = −1.4 V vs Ag/AgCl, deposition time = 300 s	1–100 μg/L	–	0.07 μg/L	–	[49]
Fe_3O_4-chitosan//GCE	0.1 M ABS	SWASV	pH = 5, deposition potential = −1.0 V vs Ag/AgCl, deposition time = 150 s	0.1–1.4 μM	50.6 μA/μM	0.0422 μM (0.0087 μg/L)	–	[131]
rGO- Fe_3O_4/GCE	0.1 M ABS	SWASV	pH = 5, deposition potential = −1.2 V vs Ag/AgCl, deposition time = 120 s	0.2–3 μM	19.13 μA/μM	6 nM (0.0012 μg/L)	2 nM (0.0004 μg/L)	[161]

Abbreviations: GCE-glassy carbon electrode, PDA-polydopamine, MnO_2 –Manganese dioxide, rGO-reduced graphene oxide, CNT-carbon nanotubes, Ppy-polypyrrole, NiO- Nickel oxide, BCN- boron carbon-nitride, Bi_2O_3 - Bismuth oxide, C_3N_4 –Carbon nitride, ZnONRs- Zinc oxide nanorods, ITOE-Indium Tin oxide electrode, ae-Fe – acid etched iron, CCE-carbon cloth electrode, SiO_2 –Silicon dioxide (silica), IIP-ion imprinted polymer, MWCNTs-multi-walled carbon nanotubes, CPE-carbon paste electrode, LSG-laser scribed graphene, CS- chitosan, G2@PAD-second generation polyamidoamine dendrime, FePc- Iron-phthalocyanine, NG-nitrogen doped graphene, ABS-acetate buffer solution, PBS-phosphate buffer solution, SWASV-square wave anodic stripping voltammetry, DPASV-Differential pulse anodic stripping voltammetry.

dearth of studies on optimization of the electrolyte concentration, and it is observed that usually a strength of 0.1 M has been immensely selected for electrochemical studies without any scientific justification.

5.1.2. Modifier volume

There is a need to optimize the amount of modifier added onto the electrode surface. This is because excess of the modifiers, especially those that are water soluble, increases the thickness of the electrode and limits the electron transfer, thus affects the sensitivity of the sensor [171]. At optimal quantities, the modifier increases the number of binding sites at the surface of the electrode resulting into increased redox currents [172]. Studies have optimized the amount/volume of iron oxide-based nanocomposites drop cast onto WEs for high sensitivity and lowest limit of detection and quantification of Pb^{2+}. The influence of the amount of Fe_3O_4@PDA@MnO_2 (0.05–0.2 mg) on the sensitivity of GCE towards Pb^{2+} was studied by Wang et al. [169] by observing changes in anodic currents. Their results indicated that current increased with increase in the amount of the modifier up to 0.1 mg owing to enhanced adsorption, above 0.1 mg, there was a tremendous reduction in current attributed to limitation of electron transfer. In another study, the concentration effect (0.2–1.6 mg/mL) of graphene oxide@polyamidoamine dendrimer@Fe_3O_4 (GO- Fe_3O_4-PAMAM/GCE) on the current signals of Pb^{2+} was studied by Baghayeri et al. [173]. The findings indicated that response current increased with increase in modifier concentration up to 1.0 mg/mL, and decreased thereafter. They ascribed the decrease in peak current at higher modifier concentration to reduction of conductive area at the electrode surface. According to Kong et al. [37], electrode surface area can as well affect the optimal amount of modifier to be added, which in turn affects the electron transfer efficiency and subsequently the detection process. The modifier properties such as surface functional groups, morphology, crystalline nature to mention a few, will greatly influence its optimal volume/concentration added onto the WE. This is because, these properties have a striking effect on the amount of Pb^{2+} adsorbed onto the electrode surface. There is thus no standard range of modifier volume recommended for modification of electrodes, and as such, it is always pertinent to optimize these quantities for each individual modifying agent. The optimal volumes for different modifiers used during voltammetric detection of Pb^{2+} in water are shown in Table 3.

5.1.3. Solution pH

The pH of the supporting electrolyte plays an immerse role in affecting the intensity of the redox currents of metals ions [128] as well as the groups on the electrode surface that will be available for complexation with these ions [85]. At lower pH values, the excess H^+ present in solution, gets adsorbed on the electrode surface and neutralizes the negative charge which in return reduces the adsorption of Pb^{2+} [174]. Similarly, the protons present in solution at lower pH compete with Pb^{2+} for the active electrode sites minimizing the amount of metal deposited on the electrode [42,168]. These phenomena thus lead to a reduction in the response peak redox currents. On the other hand, Pb^{2+} tend to hydrolyze at a higher solution pH resulting into a reduction in the accumulating ions [21]. The excess hydroxyl ions present at higher pH may complex with $Pb^{2+}$and decrease the possibility of these metal ions to complex with other groups on the electrode surface resulting into reduced detection potentials [85]. Noteworthy, the effects of higher pH (formation of metal hydroxides) are more likely to occur than those of lower pH (protonation of the electrode's functional groups). On this basis, optimization of the pH value with modified electrodes is often carried out in an acidic environments [128]. As an example, Bagherzadeh et al. [175] evaluated the influence of the pH (3 and 8) on electrochemical behavior of magnetic carbon paste electrode modified with iron oxide nanoparticles (Fe_3O_4/MCPE) in 0.1 M PBS. Their results indicated that the modified electrode exhibited a higher peak current (40.5 μA) at pH of 3 than the bare electrode (10.2 μA). This was attributed to the increased surface area and presence of hydroxyl functional groups on Fe_3O_4 that enhanced electron transfer thus increasing current. On the other hand, Fe_3O_4/MCPE showed reduced and lower peak current (10 μA) than the bare MCPE in the alkaline environment (pH = 8) attributed to increased electrostatic repulsion. The optimal solution pH values for detection of Pb^{2+} using different iron oxide-based electrodes are shown in Table 3. The pH of the supporting electrolyte also gives insights on the number of electrons and protons involved in electrochemical redox reactions by relating the obtained peak voltage through the Nernst Eq (1) [80]:

$$E_p = S.\frac{m}{n}pH + b \quad (1)$$

Where; E_p is the peak potential (mV), m and n are the number of protons and electrons in the electrochemical reaction respectively, b is the intercept of the equation, and S is the linear slope of the equation whose theoretical absolute value of 59.2 mV pH^{-1} implies that equal number of protons and electrons are involved in the reaction.

5.1.4. Scan rate

The scan rate is a key parameter in voltammetry as it indicates how fast the applied potential is passed (scanned) across the working electrode. Optimization of scan rates is often carried out at initial stages of selecting the most suitable modified electrode in terms of effective surface area, and adsorbed surface coverage. Scan rate affects the peaks of observed potential, current and width of voltammogram which in return affect selectivity, sensitivity, and limits of detection [81]. Faster scan rates result into higher peak currents, shifts in peak potential towards more positive values, and decrease in peak widths. On the other hand, slower scan rates lead to lower peak currents, shift in peak potential towards more negative values, and increased peak widths [176]. In terms of detection, slower rates are favorable for lower concentrations while faster rates suit higher concentration ranges. When an increase in the scan rate results into potential shifts of redox currents, it implies that the reaction is irreversible [177]. The relationship between peak current and scan rate can be established using the Randles- Sevcik equation (Eq 2) from which the electrode surface area is obtained. The surface area guides in selecting the most suitable working electrode for detection of the target pollutant:

$$I_p = 2.69\ x10^5 n^{3/2} D^{1/2} A C v^{1/2} \quad (2)$$

Where I_p is the peak current (A), n is the number of electrons transferred in the redox reaction, D is the diffusion coefficient ($cm^2 s^{-1}$), A is the electrode area (cm^2), C is the concentration of the redox probe used (mol cm^{-3}), and v is the scan rate (Vs^{-1})

When the redox peak currents are linearly proportional to the square root of scan rates (in a plot of peak currents vs square root of scan rates), then the electrochemical detection process is controlled by diffusion [41], and it also indicates a surface confined redox process [178]. Noteworthy, the non-existence of a zero intercept in these plots implies that electrode kinetic process is not solely controlled by diffusion rate of the analyte to the surface of the electrode [179]. The electron transfer mechanism to the electrode surface is established through the slope obtained from a plot of log of peak currents versus log of scan rates. A perfectly diffusion controlled mechanism will have a slope of 0.5 while a value between 0.5 and 1 indicates an adsorption associated process [172,180]. For an electrode adsorbed mechanism, the current response is expected to vary linearly with scan rate, and the surface coverage of the adsorbed material is calculated according to Eq (3) [81]:

$$I_p = \frac{n^2 F^2}{4RT} A \Gamma v \quad (3)$$

Where F is Faraday's constant, R is universal gas constant, T is temperature in kelvin, Γ is surface coverage, and other parameters are defined in Eq (2).

Furthermore, the adsorption phenomenon can be confirmed using the slope of a Tafel graph which is attained when peak voltage is plotted against the log of scan rate. From the same slope, the charge transfer coefficient can be obtained as shown in Eqs (4) and (5) [24]:

$$E_p = \left(\frac{b}{2}\right) \log v + constant \quad (4)$$

$$b = \frac{2.3\ RT}{(1-\alpha)nF} \quad (5)$$

Where b is the Tafel value which is the slope of Tafel plot, and α is the charge transfer co-efficient.

Tafel values are given in units of mV/dec, and values greater than 118 mV/dec signify adsorption of analytes onto the electrode [146,179,181].

5.1.5. Deposition potential and time

The deposition/accumulation potential is the potential applied to the WE to deposit (concentrate) an analyte of interest to the electrode's surface. On the hand, deposition time is the time necessary for the target analyte to interact and get fixed at the electrode surface. Almost all voltammetric studies optimize these two parameters due to their direct effects on sensitivity, and detection limits of the WEs [21]. During the detection of Pb^{2+},an optimized increase in accumulation potential (in the negative values) and time results into higher concentration of Pb^{2+}deposited onto the electrode thus translating into increased stripping peak currents and consequently increased sensitivity and low LODs. Too much negative deposition potentials and increased deposition times contribute to evolution of hydrogen which causes electrode fouling, limited available active sites, and interference of HMI adsorption resulting into reduced sensitivity witnessed by declines in stripping peak currents [45,171,182]. It is recommended to have longer accumulation potentials and times for low concentrations of Pb^{2+} [173]. Additionally, the optimal deposition potential and time will depend on the modifier and electrolyte used (Table 3)

5.1.6. Interference of other ions

In real environmental water samples, e.g., from rivers, lakes, taps, and springs, Pb^{2+} usually co-exists with other cations such as Cd^{2+}, Hg^{2+}, As^{2+}, Cu^{2+}, Mn^{2+}, Al^{3+}, Ca^{2+}, and Mg^{2+} or anions such as PO_4^{3-}, NO_3^-, SO_4^{2-}, Cl^-, Br^-. The presence of these ions can have an effect on the sensitivity and thus the detection capabilities of the electrodes. This is because these ions may co-deposit with Pb^{2+} and compete with the active sites on the WE surface causing changes in the resultant peak currents [183]. The interference effect of the ions is studied by observing the change in the redox current at optimal voltammetric conditions when the concentration of these suspected interfering species is increased a number of times as compared to that of Pb^{2+}. Therefore, the anti-interference ability of the modified electrode is one of the most crucial parameters impacting the accuracy of monitoring [169]. The tolerance limit is taken as the concentration of the interference ion that causes a relative standard error of <5 % in the observed peak currents or detection limits [24,75,134,136,184]. Alternatively, the ratio (I_I/I_O) of the currents in presence (I_I) and in absence (I_o) of interfering ion (s) is obtained, with a value of 1 indicating high anti-interference abilities of the modified electrode [154]. A number of studies have indicated that existence of different ions in concentrations of up to 500 times greater than Pb^{2+} generated no significant effect in the sensitivity and detection capabilities of iron oxide based modified electrodes [37,43,45,134,135,138]. Nevertheless, the nature of the composite materials (iron oxide-based modifiers) and the interfering ions into consideration can affect this analogy. For instance, when using Cysteine/Au@SiO_2@Fe_3O_4/NG/GCE for detection of Pb^{2+}, a 5 fold concentration of Cu^{2+}, Ag^+ and Sn^{2+} resulted into a 15 % reduction in peak current as opposed to only 5 % reduction in current when a 5 fold concentration of Zn^{2+}, Ni^{2+}, and Cd^{2+} were considered [71]. The optimal voltammetric conditions and indicator parameters (sensitivity, LODs, and LOQs) for detection of Pb^{2+} using working electrodes modified with iron oxide-based materials are shown in Table 3.

6. Sensing mechanism

When nonconductive materials such as IONPs are used in the modification of working/sensing electrodes, the detection of HMIs is depicted using an adsorption-release model as described by Liao et al. [140]. Firstly, under constant stirring, Pb^{2+} ions in water are adsorbed onto the surface of the nanomaterial, followed by desorption and diffusion onto the bare electrode surface as a result of concentration differences. On applying, the deposition potential, the ions are reduced on the electrode surface according to reaction 1. The second step involves scanning the potential from positive to negative values, so that the reduced metal is re-oxidized back to its ionic form according to reaction 2, and resulting into a stripping current signal:

Reaction 1: $Pb^{2+} + 2e \rightarrow Pb^{0}$

Reaction 2: Pb^{0} -2e $\rightarrow Pb^{2+}$

The more Pb^{2+} is adsorbed on the surface of material, the more it will be released, thus strengthening the stripping peak current responses [93,135]. It should be noted that the adsorption and desorption abilities of the electrode modifiers immensely affect the intensity of the response signals. Low desorption energy barrier indicates that the absorbed ions can be easily transferred to the electrode surface from the solution [140].

Deeper insights about the mechanism of adsorption are analyzed with various computational simulation approaches such as: Hartree-Fock calculations, Grand canonical Monte Carlo, molecular dynamics), and density functional theory (DFT). These simulations elaborate the adsorption mechanism especially at microscopic level [185] thus offering sufficient description of the kinetics and thermodynamics of the adsorption process [186]. DFT is the commonly used theory since it accounts for more details about electron and ionic interactions [187]. Additionally, DFT calculations also indicate the geometric orientation, equilibrium distance between the pollutant and the electrode, surface adsorption energy, vibration frequencies, as well as the bond length on electrode surfaces before, and after adsorption. DFT studies also indicate how the presence and interaction of different surface functional groups on the modifier influence the adsorption process [188]. As an example, Qureashi et al. [48] used the DFT theory to study and establish the interaction energies and Mulliken charges analyses for a citrate@Fe_3O_4–Pb^{2+} system. The charge analysis indicated that the negative charge on the oxygen atoms of the carboxylate group for the citrate molecule was enhanced on interaction with Pb^{2+} ions which indicated some sort of charge transfer from the metal ion to citrate. This interaction was confirmed with the UV–vis absorption spectra where an intense band in the visible region (which is the charge transfer band) was observed between citrate-Pb system, and this band was not visualized for the citrate molecule. Furthermore, the interaction energy between citrate@Fe_3O_4–Pb^{2+} system was found to be -2745.59 kJ mol^{-1}.

7. Practical application of iron oxide-based sensors in real water samples

To illustrate the potential application of the modified sensors, environmental water samples from lakes, rivers, tap, springs, and seawater are collected and subjected to voltammetric analysis under optimized conditions. The collected water samples are usually not subjected to any pretreatment apart from filtration to remove suspended solids if any. Due to the possibility of these water samples not containing detectable concentrations of Pb^{2+}, a standard addition method which involves spiking a known concentration of Pb^{2+} in multiple aliquots is adopted. After spiking, the developed sensor is used to measure the concentration in the water sample, and recovery is established by comparing the measured concentration with that which was spiked into the sample. It has been observed that iron oxide nanocomposite-based sensors show great recoveries sometimes exceeding 100 % (Table 4) which indicates good sensitivity, and accuracy of these sensors. Among the key factors considered for reliable application of electrochemical sensors are stability, reproducibility and repeatability. These terms are described in Table 1. Almost all studies that have utilized iron oxide base materials to modify sensors for voltammetric detection of Pb^{2+} have assessed these three parameters. Some of these studies and the assessment outcomes are presented in Table 5.

Table 4
Recovery studies on the use of iron oxide based electrochemical sensors on detection of Pb^{2+} in environmental water samples.

Iron oxide based working electrode[a]	Source of water	Amount of Pb^{2+} added	Amount of Pb^{2+} measured by the sensor	Recovery (%)	Country	Reference
β-cyclodextrin–NH_2– Fe_3O_4/GCE	River	0.1–0.5 μM	0.097–0.493 μM	97.0–98.6	China	[189]
Fe_3O_4@mesoporous carbon/GCE	Tap	1–2 μM	1.07–1.99 μM	99.5–107. 0	China	[43]
Fe_3O_4/Bi_2O_3/C_3N_4/GCE	River	0.1–1 μM	0.097–0.98 μM	97.8–101.1	China	[75]
rGO@CNT@Fe_2O_3/PPy/GCE	Tap	0.5–2 μM	0.487–2.035 μM	99.2–100.4	India	[136]
Fe_3O_4@PDA@MnO_2/GCE	Lake	1–20 μg/L	0.98–20.05 μg/L	98–100.8	China	[169]
NH_2–Fe_3O_4@carbon microsphere/ GCE	Tap	1.5–3.5 μM	1.53–3.71 μM	100.8–106.0	China	[72]
Fe_3O_4/MWCNTs/LSG/CS/GCE	Tap	20–30 μg/L	18.76–27.03 μg/L	97.86–99.71	China	[166]
GO@ Fe_3O_4@2-CBT/GCE	River	3.5–75	3.4–74.5	97.1–99.3	New-Zealand	[134]
L-cysteine@Au/ @SiO_2@Fe_3O_4@NG/GCE	River	0–20 μg/L	9.42–29.89 μg/L	98.1–102.35	China	[71]

[a] Abbreviations: 2-CBT-benzothiazole-2-carboxaldehyde.

Table 5
Stability, repeatability, and reproducibility results of different iron oxide based electrochemical sensors towards the detection of Pb^{2+} in water.

Iron oxide based working electrode	Studied conditions	Stability analysis	Repeatability analysis (number of successive measurements with single electrode)	Reproducibility analysis (number of electrodes for similar measurements)	Observed Relative Standard Deviation, RSD (%)			Reference
					Stability	Repeatability	Reproducibility	
Fe_3O_4/MWCNTs/LSG/CS/GCE	0.1 M PBS, 60 μg/L of Pb^{2+}, pH = 5, deposition potential = −1.2 V vs Ag/AgCl, deposition time = 150 s	Sensor stored at 4 °C for four weeks with weekly analysis	10	5	3.93	0.97	6.81	[166]
Fe_3O_4/D-valine/GCE	0.1 M ABS, 1 μM of Pb^{2+}, pH = 5.2, deposition potential = −1.1 V vs SCE deposition time = 300 s	Measurement repeated on day 16	–	10	78.04 % peak current retained		2.37	[45]
Fe_3O_4@mesoporous carbon/GCE	0.1 M ABS, 1 μM of Pb^{2+}, pH = 5, deposition potential = −1.0 V vs SCE deposition time = 150 s	–	10			2.1		[43]
ae-Fe/Fe_2O_3@CCE	0.1 M ABS, 1 μM of Pb^{2+}, pH = 4.5, deposition potential = −1.1 V vs Ag/AgCl, deposition time = 160 s	–	–	6	–	–	5.7	[40]
Fe_3O_4/GCE	0.1 M ABS, 0.5 μM of Pb^{2+}, pH = 5, deposition potential = −0.9 V vs Ag/AgCl, deposition time = 120 s		20	–	2.4	2.4		[164]
α-Fe_2O_3/BCN/Nafion/GCE	0.1 M ABS, 50 μg/L of Pb^{2+}, pH = 4, deposition potential = −1.2 V vs Ag/AgCl, deposition time = 400 s	Measurements done on day 1 and day 30 using the same sensor were compared	5	5	92 % of peak current retained on day 30	0.88	2.84	[39]
Fe_2O_3/ZnONRs/ITOE	0.1 M ABS, 0.5 μM of Pb^{2+}, pH = 5, deposition potential = −1.1 V vs Ag/AgCl, deposition time = 120 s	–	10	5		1.8	3.4	[3]
Fe_3O_4/Bi_2O_3/C_3N_4/GCE	0.1 M ABS, 0.1 μM of Pb^{2+}, pH = 4.5, deposition potential = −1.1 V vs SCE, deposition time = 300 s	Sensor stored at 4 °C and analysis done on day 15	–	10	98.9 % of peak current retained		4.2	[75]
rGO@CNT@Fe_2O_3/PPy/GCE	0.1 M ABS, 0.2 μM of Pb^{2+}, pH = 4.5, deposition potential = −1.3 V vs Ag/AgCl, deposition time = 300 s	–	5	5		2.68	4.3	[136]
N- BDMP/Fe_3O_4/IL/CPE.	0.1 M B–R, 5 nM of Pb^{2+}, pH = 3.5, deposition potential = −1.1 V vs Ag/AgCl, deposition time = 240 s	Measurements done on day 7 and day 20 using the same sensor were compared	10	10	No significant loss in current after 7 days, 8.55 % loss in current after 20 days	2.3	3.5	[142]

Abbreviations: N-BDMP-Nitro Benzoil Diphenyl Methylene Phosphorane, IL-ionic Liquid.

8. Discussions of future prospects

Unregulated anthropogenic activities such as mining, industrialization and agriculture have exacerbated the concentrations of heavy metal ions such as Pb (II) in drinking water sources to levels that are a threat to human health. Electrochemical sensors have been reliably used in timely and accurate detection of Pb^{2+} in water. The reviewed literature has proved that the performance of these sensors towards detection Pb^{2+} is improved with modification of their working electrode (WE) surfaces with iron oxide based nanocomposites. However, it has been observed that in most cases, a number of reagents/components are used to modify the surface of bare iron oxide nanoparticles (IONPs) for enhanced sensors' performance. This implies that lengthy and costly preparation pathways are involved which limit the reproducibility and sustainability of the process. As such, there is a need to explore material(s) with superior surface functional groups, many active sites, and with enhanced stability for modification of IONPs and hence WE surfaces. One such material is activated carbon from biomass materials which is characterized by high conductivity, many surface functional groups, high specific surface area and biocompatibility. However, there is limited utilization of these activated carbons alongside IONPs in modification of WEs. It is worth mentioning that steel/iron industrial wastes have been greatly used as IONPs precursors for remediation of pollutants in water [92]. Nevertheless, there is a dearth of information on the use of these steel based waste materials in generation of IONPs specifically for modification of electrochemical sensors for heavy metal ions detection. Much as all studies characterize the developed iron oxide nanoparticles in terms of morphology, functional groups, magnetic properties, crystalline nature, particle sizes, and specific surface area, limited studies have justified/quantified how these properties affect the performance of the modified electrodes in detection of Pb^{2+}, therefore, this area needs further scientific exploration. Reviewed literature has revealed that classical electrodes such as the glassy carbon electrode (GCE) are the commonly used bare electrode. However, these electrodes require frequent polishing and cleaning before and after every electrochemical application. This can limit their sensitivity and ease of operation. In addition, measurements can only be executed in presence of counter and reference electrodes. These challenges can be reduced by using screen-printed electrodes as disposable, single-shot, and reproducible bare electrodes where modifiers of interest can be embedded. It has also been observed that all the studies analyzed in this review used the "one-parameter-at-a-time" approach to select the most suitable operating conditions such as solution pH, deposition potential, deposition time, scan rate, and modifier volume. This approach is time consuming due to a number of experiments that are required and as such turns out to be costly yet the most optimal values may be missed out. The optimization process can be improved by employing tools such as response surface methodology and machine learning techniques like artificial neural network so that additional information on mass transport, kinetics and thermodynamics of the electrochemical reaction can be established. Lastly, the sustainability in terms of life cycle assessment (LCA) and economic feasibility of electrochemical sensors modified with iron oxide nanoparticles/nanocomposites need to be investigated. Performing a reliable LCA necessitates access to long term data on energy consumption, emissions, costs, and benefits throughout all stages of the life cycle of the generated modified electrodes. However, there is no published information on such data which limits a thorough LCA. Part of the sustainability plan would be establishing the regulations and standards of using the modified electrodes due to toxicological possibilities associated with poor disposal of nanomaterials in the environment.

9. Conclusions

This review highlights the recent developments in the use of iron oxide-based nanomaterials for modification of electrochemical sensors to increase sensitivity and selectivity of Pb^{2+} ions in water. It has been revealed that a number of materials can be used to increase the physical and chemical properties of bare iron oxide nanoparticles (IONPs) through surface functionalization. When the functionalized IONPs are used as modifiers of working electrodes for electrochemical sensors, they result into increased peak currents, and reduced charge transfer resistances thus improving detection capabilities towards Pb^{2+}. Square wave anodic stripping voltammetry (SWASV) and differential pulse anodic stripping voltammetry (DPASV) are the commonly used voltammetric techniques for detection of Pb^{2+} operating with electrolytes mainly in the acidic environment (pH of 3–5.6). The obtained detection limits when using IONP based electrodes have been observed to be below the existing, and the new proposed permissible limits of 10 μg/L, and 5 μg/L, respectively for Pb^{2+} in drinking water. Despite this tremendous progress in deployed of IONP based materials to modify sensors for detection of heavy metal ions specifically Pb^{2+}, there are a number of scientific gaps that need to be filled. For instance, the optimal operation parameters during voltammetric detection of Pb^{2+} can be established with simulation tools. Additionally, life cycle assessment studies can help in justifying the sustainable (environmental, economic and social acceptance) usage of iron oxide based electrochemical sensors in comparison to conventional detection techniques such as spectroscopy.

Data availability statement

No primary data was used for this review article.

CRediT authorship contribution statement

Joseph Jjagwe: Writing – original draft, Funding acquisition, Formal analysis, Conceptualization. **Peter Wilberforce Olupot:** Writing – review & editing, Supervision, Project administration, Funding acquisition. **Robinah Kulabako:** Writing – review & editing, Supervision. **Sandro Carrara:** Writing – review & editing, Supervision, Project administration, Funding acquisition, Conceptualization.

Declaration of competing interest

The authors declare that they have no known competing financial interests or personal relationships that could have appeared to influence the work reported in this paper.

Acknowledgement

This work was supported by the 100 PhDs for Africa program under the UM6P – EPFL Excellence in Africa Initiative.

References

[1] V. Priyan, N. Kumar, S. Narayanasamy, Toxicological assessment and adsorptive removal of lead (Pb) and Congo red (CR) from water by synthesized iron oxide/activated carbon (Fe3O4/AC) nanocomposite, Chemosphere 294 (2022) 133758, https://doi.org/10.1016/j.chemosphere.2022.133758.
[2] Lalhmunsiama, R.R. Pawar, S.M. Hong, K.J. Jin, S.M. Lee, Iron-oxide modified sericite alginate beads: a sustainable adsorbent for the removal of As(V) and Pb (II) from aqueous solutions, J. Mol. Liq. 240 (2017) 497–503, https://doi.org/10.1016/j.molliq.2017.05.086.
[3] H.A. Hamid, Z. Lockman, N.M. Nor, N.D. Zakaria, K.A. Razak, Sensitive detection of Pb ions by square wave anodic stripping voltammetry by using iron oxide nanoparticles decorated zinc oxide nanorods modified electrode, Mater. Chem. Phys. 273 (2021) 125148, https://doi.org/10.1016/j.matchemphys.2021.125148.
[4] J. Qu, Y. Liu, L. Cheng, Z. Jiang, G. Zhang, F. Deng, L. Wang, W. Han, Y. Zhang, Green synthesis of hydrophilic activated carbon supported sulfide nZVI for enhanced Pb(II) scavenging from water: characterization, kinetics, isotherms and mechanisms, J. Hazard Mater. 403 (2021) 123607, https://doi.org/10.1016/j.jhazmat.2020.123607.
[5] C. Nyambura, N.O. Hashim, M.W. Chege, S. Tokonami, F.W. Omonya, Cancer and non-cancer health risks from carcinogenic heavy metal exposures in underground water from Kilimambogo, Kenya, Groundw. Sustain. Dev. 10 (2020) 100315, https://doi.org/10.1016/j.gsd.2019.100315.
[6] A. Pranudta, N. Chanthapon, P. Kidkhunthod, M.M. El-Moselhy, T.T. Nguyen, S. Padungthon, Selective removal of Pb from lead-acid battery wastewater using hybrid gel cation exchanger loaded with hydrated iron oxide nanoparticles: fabrication, characterization, and pilot-scale validation, J. Environ. Chem. Eng. 9 (2021) 106282, https://doi.org/10.1016/j.jece.2021.106282.
[7] G. Sarojini, S. Venkateshbabu, M. Rajasimman, Facile synthesis and characterization of polypyrrole - iron oxide – seaweed (PPy-Fe3O4-SW) nanocomposite and its exploration for adsorptive removal of Pb(II) from heavy metal bearing water, Chemosphere 278 (2021) 130400, https://doi.org/10.1016/j.chemosphere.2021.130400.
[8] J.M. Bloor, R.D. Handy, S.A. Awan, D.F.L. Jenkins, Graphene oxide biopolymer aerogels for the removal of lead from drinking water using a novel nano-enhanced ion exchange cascade, Ecotoxicol. Environ. Saf. 208 (2021) 111422, https://doi.org/10.1016/j.ecoenv.2020.111422.
[9] R. Bhateria, R. Singh, A review on nanotechnological application of magnetic iron oxides for heavy metal removal, J. Water Process Eng. 31 (2019) 100845, https://doi.org/10.1016/j.jwpe.2019.100845.
[10] R.R. PawarLalhmunsiama, M. Kim, J.G. Kim, S.M. Hong, S.Y. Sawant, S.M. Lee, Efficient removal of hazardous lead, cadmium, and arsenic from aqueous environment by iron oxide modified clay-activated carbon composite beads, Appl. Clay Sci. 162 (2018) 339–350, https://doi.org/10.1016/j.clay.2018.06.014.
[11] M. Ghanei-Motlagh, M. Fayazi, M.A. Taher, E. Darezereshki, E. Jamalizadeh, R. Fayazi, Novel modified magnetic nanocomposite for determination of trace amounts of lead ions, RSC Adv. 5 (2015) 100039–100048, https://doi.org/10.1039/c5ra20705c.
[12] M.J. Gibson, M. Fisher, A. Clonch, J.M. MacDonald, P.J. Cook, Children drinking private well water have higher blood lead than those with city water, Proc. Natl. Acad. Sci. U.S.A. 117 (2020) 16898–16907, https://doi.org/10.1073/pnas.2002729117.
[13] WHO, Lead in drinking water: background document for development of WHO Guidelines for drinking-water quality, WHO/FWC/WSH/16.53. WHO/SDE/WS (2016) 1–27. https://cdn.who.int/media/docs/default-source/wash-documents/wash-chemicals/lead-background-feb17.pdf?sfvrsn=fc50727b_4. (Accessed 22 January 2023).
[14] R. Meng, Q. Zhu, T. Long, X. He, Z. Luo, R. Gu, W. Wang, P. Xiang, The innovative and accurate detection of heavy metals in foods: a critical review on electrochemical sensors, Food Control 150 (2023) 109743, https://doi.org/10.1016/j.foodcont.2023.109743.
[15] C.J. Mei, A.A.A. Shahrul, A review on the determination heavy metals ions using calixarene-based electrochemical sensors, Arab. J. Chem. 14 (2021) 103303, https://doi.org/10.1016/j.arabjc.2021.103303.
[16] M.M. Langari, M.M. Antxustegi, J. Labidi, Nanocellulose-based sensing platforms for heavy metal ions detection: a comprehensive review, Chemosphere 302 (2022) 134823, https://doi.org/10.1016/j.chemosphere.2022.134823.
[17] J. Baranwal, B. Barse, G. Gatto, G. Broncova, A. Kumar, Electrochemical sensors and their applications: a review, Chemosensors 10 (2022), https://doi.org/10.3390/chemosensors10090363.
[18] A. Barhoum, S. Hamimed, H. Slimi, A. Othmani, F.M. Abdel-Haleem, M. Bechelany, Modern designs of electrochemical sensor platforms for environmental analyses: principles, nanofabrication opportunities, and challenges, Trends Environ. Anal. Chem. 38 (2023) e00199, https://doi.org/10.1016/j.teac.2023.e00199.
[19] T.H. Kim, Advanced Electrochemical Biosensors, 2021.
[20] A. Waheed, M. Mansha, N. Ullah, Nanomaterials-based electrochemical detection of heavy metals in water: current status, challenges and future direction, TrAC, Trends Anal. Chem. 105 (2018) 37–51, https://doi.org/10.1016/j.trac.2018.04.012.
[21] Y. Lu, X. Liang, C. Niyungeko, J. Zhou, J. Xu, G. Tian, A review of the identi fi cation and detection of heavy metal ions in the environment by voltammetry, Talanta 178 (2018) 324–338, https://doi.org/10.1016/j.talanta.2017.08.033.
[22] I.G. David, M. Buleandra, D.E. Popa, M.C. Cheregi, E.E. Iorgulescu, Past and present of electrochemical sensors and methods for Amphenicol Antibiotic analysis, Micromachines 13 (2022), https://doi.org/10.3390/mi13050677.
[23] S. Ren, J. Zeng, Z. Zheng, H. Shi, Perspective and application of modified electrode material technology in electrochemical voltammetric sensors for analysis and detection of illicit drugs, Sensors Actuators, A Phys. 329 (2021) 112821, https://doi.org/10.1016/j.sna.2021.112821.
[24] S. Tajik, H. Beitollahi, H.W. Jang, M. Shokouhimehr, A screen printed electrode modified with Fe3O4@polypyrrole-Pt core-shell nanoparticles for electrochemical detection of 6-mercaptopurine and 6-thioguanine, Talanta 232 (2021) 122379, https://doi.org/10.1016/j.talanta.2021.122379.
[25] F. Laghrib, M. Bakasse, S. Lahrich, M.A. El Mhammedi, Electrochemical sensors for improved detection of paraquat in food samples: a review, Mater. Sci. Eng., C 107 (2020) 110349, https://doi.org/10.1016/j.msec.2019.110349.
[26] Y. Shen, H. Ouyang, W. Li, Y. Long, Defect-enhanced electrochemical property of h-BN for Pb2+ detection, Microchim. Acta 188 (2021), https://doi.org/10.1007/s00604-020-04691-z.
[27] T.S. Munonde, P.N. Nomngongo, Nanocomposites for electrochemical sensors and their applications on the detection of trace metals in environmental water samples, Sensors 21 (2021) 1–27, https://doi.org/10.3390/s21010131.
[28] M. Fayazi, G.-M. Masoud, K. Changiz, Application of magnetic nanoparticles modified with L-cysteine for pre-concentration and voltammetric detection of copper (II), Microchem. J. 181 (2022) 107652, https://doi.org/10.1016/j.microc.2022.107652.
[29] F. Mollarasouli, E. Zor, G. Ozcelikay, S.A. Ozkan, Magnetic nanoparticles in developing electrochemical sensors for pharmaceutical and biomedical applications, Talanta 226 (2021) 122108, https://doi.org/10.1016/j.talanta.2021.122108.

[30] A. Hayat, A. Rhouati, R.K. Mishra, G.A. Alonso, M. Nasir, G. Istamboulie, J.L. Marty, An electrochemical sensor based on TiO2/activated carbon nanocomposite modified screen printed electrode and its performance for phenolic compounds detection in water samples, Int. J. Environ. Anal. Chem. 96 (2016) 237–246, https://doi.org/10.1080/03067319.2015.1137910.

[31] G. Maduraiveeran, W. Jin, Nanomaterials based electrochemical sensor and biosensor platforms for environmental applications, Trends Environ. Anal. Chem. 13 (2017) 10–23, https://doi.org/10.1016/j.teac.2017.02.001.

[32] A.V. Bounegru, C. Apetrei, Carbonaceous nanomaterials employed in the development of electrochemical sensors based on screen-printing technique—a review, Catalysts 10 (2020), https://doi.org/10.3390/catal10060680.

[33] S. Sawan, R. Maalouf, A. Errachid, N. Jaffrezic-Renault, Metal and metal oxide nanoparticles in the voltammetric detection of heavy metals: a review, TrAC, Trends Anal. Chem. 131 (2020) 116014, https://doi.org/10.1016/j.trac.2020.116014.

[34] M. Adampourezare, M. Hasanzadeh, M.A. Hoseinpourefeizi, F. Seidi, Iron/iron oxide-based magneto-electrochemical sensors/biosensors for ensuring food safety: recent progress and challenges in environmental protection, RSC Adv. 13 (2023) 12760–12780, https://doi.org/10.1039/d2ra07415j.

[35] W. Sheng, Q. Xu, J. Chen, H. Wang, Z. Ying, R. Gao, X. Zheng, X. Zhao, Electrochemical sensing of hydrogen peroxide using nitrogen-doped graphene/porous iron oxide nanorod composite, Mater. Lett. 235 (2019) 137–140, https://doi.org/10.1016/j.matlet.2018.10.022.

[36] K.D. Kumar, K. Raghava Reddy, V. Sadhu, N.P. Shetti, C. Venkata Reddy, R.S. Chouhan, S. Naveen, Metal Oxide-Based Nanosensors for Healthcare and Environmental Applications, INC, 2020, https://doi.org/10.1016/b978-0-12-817923-9.00004-3.

[37] Y. Kong, T. Wu, D. Wu, Y. Zhang, Y. Wang, B. Du, Q. Wei, An electrochemical sensor based on Fe3O4@PANI nanocomposites for sensitive detection of Pb2+ and Cd2+, Anal. Methods 10 (2018) 4784–4792, https://doi.org/10.1039/c8ay01245h.

[38] A.S. Agnihotri, A. Varghese, M. Nidhin, Transition metal oxides in electrochemical and bio sensing : a state-of-art review, Appl. Surf. Sci. Adv. 4 (2021), https://doi.org/10.1016/j.apsadv.2021.100072.

[39] Y. Zhu, X. Wang, P. Wang, J. Zhu, Y. He, X. Jia, F. Chang, H. Wang, G. Hu, Two-dimensional BCN nanosheets self-assembled with hematite nanocrystals for sensitively detecting trace toxic Pb(II) ions in natural water, Ecotoxicol. Environ. Saf. 225 (2021), https://doi.org/10.1016/j.ecoenv.2021.112745.

[40] F. Zhu, H. Shi, Z. Yu, C. Wang, W. Cheng, X. Zhou, F. Yang, Y. Zhang, X. Zhang, Acid-etched Fe/Fe2O3 nanoparticles encapsulated into carbon cloth as a novel voltammetric sensor for the simultaneous detection of Cd2+ and Pb2, Analyst (2020), https://doi.org/10.1039/d0an01861a.

[41] V.N. Palakollu, T.E. Chiwunze, C. Liu, R. Karpoormath, Electrochemical sensitive determination of acetaminophen in pharmaceutical formulations at iron oxide/graphene composite modified electrode, Arab. J. Chem. 13 (2020) 4350–4357, https://doi.org/10.1016/j.arabjc.2019.08.001.

[42] B. Maleki, M. Baghayeri, M. Ghanei-Motlagh, F. Mohammadi Zonoz, A. Amiri, F. Hajizadeh, A.R. Hosseinifar, E. Esmaeilnezhad, Polyamidoamine dendrimer functionalized iron oxide nanoparticles for simultaneous electrochemical detection of Pb 2+ and Cd 2+ ions in environmental waters, Meas, J. Int. Meas. Confed. 140 (2019) 81–88, https://doi.org/10.1016/j.measurement.2019.03.052.

[43] Y. Liu, S. Wu, W. Xiong, H. Li, Interface Co-Assembly synthesis of magnetic Fe3O4@mesoporous carbon for efficient electrochemical detection of Hg(II) and Pb (II), Adv. Mater. Interfac. 10 (2023) 1–12, https://doi.org/10.1002/admi.202201631.

[44] A. Kulpa, J. Ryl, G. Schroeder, A. Koterwa, J.S. Anand, T. Ossowski, P. Niedzia, Simultaneous voltammetric determination of Cd 2 + , Pb2+ , and Cu 2 + ions captured by Fe 3 O 4 @ SiO 2 core-shell nanostructures of various outer amino chain length, J. Mol. Liq. 314 (2020), https://doi.org/10.1016/j.molliq.2020.113677.

[45] M.K.S. Kumara, D.H. Nagaraju, Z. Yhobu, H.N. Nayan Kumar, S. Budagumpi, S. Kumar Bose, P. Shivakumar, V.N. Palakollu, Tuning the surface functionality of Fe3O4 for sensitive and selective detection of heavy metal ions, Sensors 22 (2022) 1–11, https://doi.org/10.3390/s22228895.

[46] S. Sawan, K. Hamze, A. Youssef, R. Boukarroum, K. Bouhadir, A. Errachid, Voltammetric study of the affinity of divalent heavy metals for guanine - functionalized iron oxide nanoparticles, Monatshefte Für Chemie - Chem. Mon. 152 (2021) 229–240, https://doi.org/10.1007/s00706-021-02738-2.

[47] J. Wei, J. Zhao, C. Li, X. Xie, Y. Wei, W. Shen, J. Wang, M. Yang, Chemical Highly sensitive and selective electrochemical detection of Pb (II) in serum via an α -Fe 2 O 3/NiO heterostructure : evidence from theoretical calculations and adsorption investigation, Sensor. Actuator. B Chem. 344 (2021) 130295, https://doi.org/10.1016/j.snb.2021.130295.

[48] A. Qureashi, A. Hussain, A. Bashir, T. Manzoor, L. Ahmad, F.A. Sheikh, Citrate coated magnetite : a complete magneto dielectric , electrochemical and DFT study for detection and removal of heavy metal ions, Surface. Interfac. 23 (2021) 101004, https://doi.org/10.1016/j.surfin.2021.101004.

[49] S. Lee, J. Oh, D. Kim, Y. Piao, A sensitive electrochemical sensor using an iron oxide/graphene composite for the simultaneous detection of heavy metal ions, Talanta 160 (2016) 528–536, https://doi.org/10.1016/j.talanta.2016.07.034.

[50] H. Han, D. Pan, Voltammetric methods for speciation analysis of trace metals in natural waters, Trends Environ. Anal. Chem. 29 (2021) e00119, https://doi.org/10.1016/j.teac.2021.e00119.

[51] P. Bijesh, V. Selvaraj, V. Andal, A review on synthesis and applications of nano metal Oxide/porous carbon composite, Mater. Today Proc. 55 (2021) 212–219, https://doi.org/10.1016/j.matpr.2021.06.163.

[52] A. Rubino, R. Queirós, Electrochemical determination of heavy metal ions applying screen-printed electrodes based sensors. A review on water and environmental samples analysis, Talanta Open 7 (2023) 100203, https://doi.org/10.1016/j.talo.2023.100203.

[53] O. Kanoun, T. Lazarević-Pašti, I. Pašti, S. Nasraoui, M. Talbi, A. Brahem, A. Adiraju, E. Sheremet, R.D. Rodriguez, M. Ben Ali, A. Al-Hamry, A review of nanocomposite-modified electrochemical sensors for water quality monitoring, Sensors 21 (2021), https://doi.org/10.3390/s21124131.

[54] W. Yang, H. Guo, R. Xue, X. Zhao, Q. Guan, T. Fan, L. Zhang, F. Yang, W. Yang, 0.2CNT/NiSex composite derived from CNT/MOF-74 as electrode material for electrochemical capacitor and electrochemical sensor, Microchem. J. 168 (2021) 106519, https://doi.org/10.1016/j.microc.2021.106519.

[55] R. Konwarh, G. Gollavelli, S.B. Palanisamy, Designing of Novel Nanosensors for Environmental Aspects, Elsevier Inc., 2020, https://doi.org/10.1016/b978-0-12-820702-4.00003-9.

[56] M.R. Akanda, A. Bibi, M.A. Aziz, Recent advances in the use of biomass-derived activated carbon as an electrode material for electroanalysis, ChemistrySelect 6 (2021) 6714–6732, https://doi.org/10.1002/slct.202101010.

[57] M. Chaudhary, A. Kumar, A. Devi, B.P. Singh, B.D. Malhotra, K. Singhal, S. Shukla, S. Ponnada, R.K. Sharma, C.A. Vega-Olivencia, S. Tyagi, R. Singhal, Prospects of nanostructure-based electrochemical sensors for drug detection: a review, Mater. Adv. 4 (2023) 432–457, https://doi.org/10.1039/d2ma00896c.

[58] G. Balkourani, A. Brouzgou, M. Archonti, N. Papandrianos, S. Song, P. Tsiakaras, Emerging materials for the electrochemical detection of COVID-19, J. Electroanal. Chem. 893 (2021) 115289, https://doi.org/10.1016/j.jelechem.2021.115289.

[59] Z. Mohammadi, S.M. Jafari, Detection of food spoilage and adulteration by novel nanomaterial-based sensors, Adv. Colloid Interface Sci. 286 (2020) 102297, https://doi.org/10.1016/j.cis.2020.102297.

[60] T. Tang, M. Zhou, J. Lv, H. Cheng, H. Wang, D. Qin, G. Hu, X. Liu, Biointerfaces Sensitive and selective electrochemical determination of uric acid in urine based on ultrasmall iron oxide nanoparticles decorated urchin-like nitrogen-doped carbon, Colloids Surf. B Biointerfaces 216 (2022) 112538, https://doi.org/10.1016/j.colsurfb.2022.112538.

[61] A.C. Lazanas, M.I. Prodromidis, Electrochemical impedance Spectroscopy—A tutorial, ACS Meas. Sci. Au. 3 (2023) 162–193, https://doi.org/10.1021/acsmeasuresciau.2c00070.

[62] J. Zhang, S. Wang, K. Ono, Electrochemical impedance spectroscopy, Microsc. Microanal. Lithium-Ion Batter (2023) 301–350, https://doi.org/10.1201/9781003299295-11.

[63] I. Tiwari, M. Singh, C.M. Pandey, G. Sumana, Electrochemical genosensor based on graphene oxide modified iron oxide-chitosan hybrid nanocomposite for pathogen detection, Sensor. Actuator. B Chem. 206 (2015) 276–283, https://doi.org/10.1016/j.snb.2014.09.056.

[64] M.M. Vinay, N.Y. Arthoba, Iron oxide (Fe2O3) nanoparticles modified carbon paste electrode as an advanced material for electrochemical investigation of paracetamol and dopamine, J. Sci. Adv. Mater. Devices. 4 (2019) 442–450, https://doi.org/10.1016/j.jsamd.2019.07.006.

[65] X. Zheng, S. Khaoulani, N. Ktari, M. Lo, A.M. Khalil, C. Zerrouki, N. Fourati, M.M. Chehimi, Towards clean and safe water: a review on the emerging role of imprinted polymer-based electrochemical sensors, Sensors 21 (2021) 1–42, https://doi.org/10.3390/s21134300.

[66] P. Devi, C. Sharma, P. Kumar, M. Kumar, B.K.S. Bansod, M.K. Nayak, M.L. Singla, Selective electrochemical sensing for arsenite using rGO/Fe 3 O 4 nanocomposites, J. Hazard Mater. 322 (2017) 85–94, https://doi.org/10.1016/j.jhazmat.2016.02.066.

[67] H. Hu, Y. Hu, B. Xie, J. Zhu, High sensitivity electrochemical as (III) sensor based on Fe3O4/MoS2 nanocomposites, Nanomaterials 13 (2023), https://doi.org/10.3390/nano13162288.

[68] R. Karthik, S. Thambidurai, Synthesis of cobalt doped ZnO/reduced graphene oxide nanorods as active material for heavy metal ions sensor and antibacterial activity, J. Alloys Compd. (2017), https://doi.org/10.1016/j.jallcom.2017.04.298.

[69] A. Moutcine, C. Laghlimi, O. Ifguis, M.A. Smaini, S.E. El Qouatli, M. Hammi, A. Chtaini, A novel carbon paste electrode modified by NP-Al2O3 for the electrochemical simultaneous detection of Pb (II) and Hg (II), Diam. Relat. Mater. 104 (2020) 107747, https://doi.org/10.1016/j.diamond.2020.107747.

[70] Y. Cai, B. Ren, C. Peng, C. Zhang, X. Wei, Highly sensitive and selective fluorescence "turn-on" detection of Pb (II) based on Fe3O4@Au–fitc nanocomposite yina, Molecules 26 (2021), https://doi.org/10.3390/molecules26113180Academic.

[71] J. Nie, B. He, Y. Cheng, W. Yin, C. Hou, D. Huo, L. Qian, Y. Qin, H. Fa, Design of L-cysteine functionalized Au@SiO2@Fe3O4/nitrogen-doped graphene nanocomposite and its application in electrochemical detection of Pb2+, Chem. Res. Chin. Univ. 33 (2017) 951–957, https://doi.org/10.1007/s40242-017-7101-2.

[72] F. Bai, X. Zhang, X. Hou, H. Liu, J. Chen, T. Yang, Individual and simultaneous voltammetric determination of Cd(II), Cu(II) and Pb(II) applying amino functionalized Fe3O4@Carbon microspheres modified electrode, Electroanalysis 31 (2019) 1465–1474, https://doi.org/10.1002/elan.201900234.

[73] J. Mei, Z. Ying, W. Sheng, J. Chen, J. Xu, P. Zheng, A sensitive and selective electrochemical sensor for the simultaneous determination of trace Cd2+ and Pb2+, Chem. Pap. 74 (2020) 1027–1037, https://doi.org/10.1007/s11696-019-00942-3.

[74] B. He, X. feng Shen, J. Nie, X. li Wang, F. mei Liu, W. Yin, C. jun Hou, D. qun Huo, H. bao Fa, Electrochemical sensor using graphene/Fe3O4 nanosheets functionalized with garlic extract for the detection of lead ion, J. Solid State Electrochem. 22 (2018) 3515–3525, https://doi.org/10.1007/s10008-018-4041-9.

[75] Y. Pu, Y. Wu, Z. Yu, L. Lu, X. Wang, Simultaneous determination of Cd2+ and Pb2+ by an electrochemical sensor based on Fe3O4/Bi2O3/C3N4 nanocomposites, Talanta Open 3 (2021) 100024, https://doi.org/10.1016/j.talo.2020.100024.

[76] B.Y. Chang, S.M. Park, Electrochemical impedance spectroscopy, Annu. Rev. Anal. Chem. 3 (2010) 207–229, https://doi.org/10.1146/annurev.anchem.012809.102211.

[77] E. Cesewski, B.N. Johnson, Electrochemical biosensors for pathogen detection, Biosens. Bioelectron. 159 (2020) 112214, https://doi.org/10.1016/j.bios.2020.112214.

[78] A. Serrà, J. García-Torres, Electrochemistry: a basic and powerful tool for micro- and nanomotor fabrication and characterization, Appl. Mater. Today 22 (2021), https://doi.org/10.1016/j.apmt.2021.100939.

[79] M.N. Nor, N.H. Ramli, H. Poobalan, K. Qi Tan, K. Abdul Razak, Recent advancement in disposable electrode modified with nanomaterials for electrochemical heavy metal sensors, Crit. Rev. Anal. Chem. 53 (2023) 253–288, https://doi.org/10.1080/10408347.2021.1950521.

[80] A.J. Bard, L.R. Faulkner, H.S. White, Electrochemical Methods: Fundamentals and Applications, third ed., John Wiley & sons, Oxford, UK, 2022.

[81] N. Elgrishi, K.J. Rountree, B.D. McCarthy, E.S. Rountree, T.T.E.J.L. Dempsey, A practical beginner ' s guide to cyclic voltammetry, J. Chem. Educ. 95 (2018) 197–206, https://doi.org/10.1021/acs.jchemed.7b00361.

[82] G. Bontempelli, N. Dossi, R. Toniolo, Voltammetry polarography, in: third ed., in: M. WorsfoldP, A. Townshend, C.F. Poole, Miró (Eds.), Encycl. Anal. Sci., Academic Press, Oxford, 2019, pp. 218–229.

[83] R. Yadav, A.N. Berlina, A.V. Zherdev, M.S. Gaur, B.B. Dzantiev, Rapid and selective electrochemical detection of pb2+ ions using aptamer-conjugated alloy nanoparticles, SN Appl. Sci. 2 (2020) 1–11, https://doi.org/10.1007/s42452-020-03840-6.

[84] Y. Uchida, E. Kätelhön, R.G. Compton, Linear sweep voltammetry with non-triangular waveforms : new opportunities in electroanalysis, J. Electroanal. Chem. 818 (2018) 140–148, https://doi.org/10.1016/j.jelechem.2018.04.028.

[85] V.H.B. Oliveira, F. Rechotnek, E.P. da Silva, V. de S. Marques, A.F. Rubira, R. Silva, S.A. Lourenço, E.C. Muniz, A sensitive electrochemical sensor for Pb2+ ions based on ZnO nanofibers functionalized by L-cysteine, J. Mol. Liq. 309 (2020) 113041, https://doi.org/10.1016/j.molliq.2020.113041.

[86] G.-M.A. Ferrari, P. Carrington, S.J. Rowley-Neale, C.E. Banks, Recent advances in portable heavy metal electrochemical sensing platforms, Environ. Sci. Water Res. Technol. 6 (2020) 2676–2690, https://doi.org/10.1039/d0ew00407c.

[87] T. Zhang, H. Jin, Y. Fang, J.B. Guan, S.J. Ma, Y. Pan, M. Zhang, H. Zhu, X.D. Liu, M.L. Du, Detection of trace Cd 2+ , Pb 2+ and Cu 2+ ions via porous activated carbon supported palladium nanoparticles modified electrodes using SWASV, Mater. Chem. Phys. 225 (2019) 433–442, https://doi.org/10.1016/j.matchemphys.2019.01.010.

[88] N.H. Abdullah, K. Shameli, E.C. Abdullah, L.C. Abdullah, Solid matrices for fabrication of magnetic iron oxide nanocomposites: synthesis, properties, and application for the adsorption of heavy metal ions and dyes, Composites, Part B 162 (2019) 538–568, https://doi.org/10.1016/j.compositesb.2018.12.075.

[89] A.G. Leonel, A.A.P. Mansur, H.S. Mansur, Advanced functional nanostructures based on magnetic iron oxide nanomaterials for water remediation: a review, Water Res. 190 (2021) 116693, https://doi.org/10.1016/j.watres.2020.116693.

[90] S.M. Devi, A. Nivetha, I. Prabha, Superparamagnetic properties and significant applications of iron oxide nanoparticles for astonishing efficacy—a review, J. Supercond. Nov. Magnetism 32 (2019) 127–144, https://doi.org/10.1007/s10948-018-4929-8.

[91] S.A. Jayanthi, D.M. Gnana, T. Nathan, J. Jayashainy, P. Sagayaraj, A novel hydrothermal approach for synthesizing a-Fe2O3, g-Fe2O3 and Fe3O4 mesoporous magnetic nanoparticles, Mater. Chem. Phys. 162 (2015) 316–325, https://doi.org/10.1016/j.matchemphys.2015.05.073.

[92] J. Jjagwe, P.W. Olupot, S. Carrara, Iron oxide nanoparticles/nanocomposites derived from steel and iron wastes for water treatment: a review, J. Environ. Manag. 343 (2023) 118236, https://doi.org/10.1016/j.jenvman.2023.118236.

[93] S. Li, W. Li, T. Jiang, Z. Liu, X. Chen, H. Cong, J. Liu, Y. Huang, L. Li, X. Huang, Iron oxide with different crystal phases (# - and # -Fe2O3) in electroanalysis and ultra-sensitive and selective detection of lead (II): an advancing approach using XPS and EXAFS, Anal. Chem. (2015), https://doi.org/10.1021/acs.analchem.5b03570.

[94] S. Sang, H. Zhang, Y. Sun, A. Jian, W. Zhang, Facile synthesis of carbon-encapsulated Fe3O4 core/shell nanospheres for application in Pb(II) electrochemical determination, Int. J. Electrochem. Sci. 12 (2017) 1306–1317, https://doi.org/10.20964/2017.02.28.

[95] S. Natarajan, K. Harini, G.P. Gajula, B. Sarmento, M. Teresa, N. Petersen, V. Thiagarajan, Multifunctional magnetic iron oxide nanoparticles : diverse synthetic approaches , surface modifications , cytotoxicity towards biomedical and industrial applications, BMC Mater (2019) 1–22, https://doi.org/10.1186/s42833-019-0002-6.

[96] S. Zhao, X. Yu, Y. Qian, W. Chen, J. Shen, Multifunctional magnetic iron oxide nanoparticles: an advanced platform for cancer theranostics, Theranostics 10 (2020) 6278–6309, https://doi.org/10.7150/thno.42564.

[97] A. Ali, H. Zafar, M. Zia, I. ul Haq, A.R. Phull, J.S. Ali, A. Hussain, Synthesis, characterization, applications, and challenges of iron oxide nanoparticles, Nanotechnol. Sci. Appl. 9 (2016) 49–67, https://doi.org/10.2147/NSA.S99986.

[98] S.P. Mardikar, V.R. Doss, P.D. Jolhe, R.W. Gaikwad, S.S. Barkade, Nanocomposite Adsorbent-Based Wastewater Treatment Processes: Special Emphasis on Surface-Engineered Iron Oxide Nanohybrids, Elsevier Inc., 2021, https://doi.org/10.1016/B978-0-12-821496-1.00025-8.

[99] M. Bilal, H.M.N. Iqbal, S.F. Adil, M.R. Shaik, A. Abdelgawad, M.R. Hatshan, M. Khan, Surface-coated magnetic nanostructured materials for robust bio-catalysis and biomedical applications-A review, J. Adv. Res. 38 (2022) 157–177, https://doi.org/10.1016/j.jare.2021.09.013.

[100] M. Yusefi, K. Shameli, A.F. Jumaat, Preparation and properties of magnetic iron oxide nanoparticles for biomedical applications : a brief review, J. Adv. Res. Mater. Sci. 1 (2020) 10–18.

[101] W. Zhang, B. Lu, H. Tang, J. Zhao, Q. Cai, Reclamation of acid pickling waste: a facile route for preparation of single-phase Fe3O4 nanoparticle, J. Magn. Magn Mater. 381 (2015) 401–404, https://doi.org/10.1016/j.jmmm.2015.01.037.

[102] A. Yakar, A. Ünlü, T. Yeşilçayır, İ. Bıyık, Kinetics and thermodynamics of textile dye removal by adsorption onto iron oxide nanoparticles, Nanotechnol. Environ. Eng. 5 (2020) 1–12, https://doi.org/10.1007/s41204-020-0068-0.

[103] S. Gyergyek, D. Makovec, M. Jagodič, M. Drofenik, K. Schenk, O. Jordan, J. Kovač, G. Dražič, H. Hofmann, Hydrothermal growth of iron oxide NPs with a uniform size distribution for magnetically induced hyperthermia: structural, colloidal and magnetic properties, J. Alloys Compd. (2016), https://doi.org/10.1016/j.jallcom.2016.09.238.

[104] P. Punia, M.K. Bharti, S. Chalia, R. Dhar, B. Ravelo, P. Thakur, A. Thakur, Recent advances in synthesis, characterization, and applications of nanoparticles for contaminated water treatment- A review, Ceram. Int. 47 (2021) 1526–1550, https://doi.org/10.1016/j.ceramint.2020.09.050.

[105] O.A. Noqta, A.A. Aziz, I.A. Usman, M. Bououdina, Recent advances in iron oxide nanoparticles (IONPs): synthesis and surface modification for biomedical applications, J. Supercond. Nov. Magnetism (2019) 779–795, https://doi.org/10.1007/s10948-018-4939-6.

[106] M.A. Sharifah, B. Abdul, Sol – gel synthesis of a -Fe_2O_3 nanoparticles and its photocatalytic application, J. Sol. Gel Sci. Technol. (2015), https://doi.org/10.1007/s10971-015-3663-y.

[107] T. Shrividhya, S. Nandhavelu, D. Vikraman, Facile methodology of sol-gel synthesis for metal oxide nanostructures, in: Facile Methodol. Sol-Gel Synth. Met. Oxide Nanostructures, 2017, pp. 1–16, https://doi.org/10.5772/intechopen.68708.

[108] E. Alzahrani, A. Sharfalddin, M. Alamodi, Microwave-hydrothermal synthesis of ferric oxide doped with cobalt, Adv. Nanoparticles (2015) 53–60.

[109] L.F. Gorup, L.H. Amorin, E.R. Camargo, T. Sequinel, F.H. Cincotto, G. Biasotto, N. Ramesar, F. de A. La Porta, Methods for Design and Fabrication of Nanosensors: the Case of ZnO-Based Nanosensor, Nanosensors for Smart Cities, 2020, pp. 9–30, https://doi.org/10.1016/b978-0-12-819870-4.00002-5.

[110] Y.L. Pang, S. Lim, H.C. Ong, W.T. Chong, Research progress on iron oxide-based magnetic materials: synthesis techniques and photocatalytic applications, Ceram. Int. 42 (2016) 9–34, https://doi.org/10.1016/j.ceramint.2015.08.144.

[111] M. Su, C. He, K. Shih, Facile synthesis of morphology and size-controlled α -Fe 2 O 3 and Fe_3 O_4 nano-and microstructures by hydrothermal/solvothermal process : the roles of reaction medium and urea dose, Ceram. Int. (2016) 1–12, https://doi.org/10.1016/j.ceramint.2016.06.111.

[112] N. Torres-gómez, O. Nava, L. Argueta-figueroa, R. García-contreras, A. Baeza-barrera, A.R. Vilchis-nestor, Shape tuning of magnetite nanoparticles obtained by hydrothermal synthesis : effect of temperature, J. Nanomater. 2019 (2019), https://doi.org/10.1155/2019/7921273.

[113] T. Ahmad, R. Phul, Magnetic iron oxide nanoparticles as contrast agents : hydrothermal synthesis , characterization and properties, Solid State Phenom. 232 (2015) 111–145, https://doi.org/10.4028/www.scientific.net/SSP.232.111.

[114] A. Mohamed, H. Shadi, M.A. Kamaruddin, N.M. Niza, M.I. Emmanuel, S. Hossain, N. Ismail, Efficient treatment of raw leachate using magnetic ore iron oxide nanoparticles Fe ₂ O ₃ as nanoadsorbents, J. Water Process Eng. 38 (2020) 101637, https://doi.org/10.1016/j.jwpe.2020.101637.

[115] I. Ali, C. Peng, D. Lin, D.P. Saroj, I. Naz, Z.M. Khan, M. Sultan, M. Ali, Encapsulated green magnetic nanoparticles for the removal of toxic Pb 2 + and Cd 2 + from water : development , characterization and application, J. Environ. Manag. 234 (2019) 273–289, https://doi.org/10.1016/j.jenvman.2018.12.112.

[116] P.C. Jikar, N.B. Dhokey, P.P. Deshpande, A.A. Bhopale, Synthesis, characterization and corrosion protection performance of nano-scale red pigment of (A-Fe2o3) hematite obtained by cryogenic mechanical milling of mill scale, SSRN Electron. J. (2022) 1–15, https://doi.org/10.2139/ssrn.4017233.

[117] A.M. Predescu, E. Matei, A.C. Berbecaru, M. Râpă, M.G. Sohaciu, C. Predescu, R. Vidu, An innovative method of converting ferrous mill scale wastes into superparamagnetic nanoadsorbents for water decontamination, Materials 14 (2021), https://doi.org/10.3390/ma14102539.

[118] S. Phearom, M.K. Shahid, Y.-G. Choi, Optimization of arsenic adsorption by mill scale–derived magnetite particles using response surface methodology, J. Hazardous, Toxic, Radioact. Waste 25 (2021) 04021022, https://doi.org/10.1061/(asce)hz.2153-5515.0000620.

[119] N.A.A. Nazri, R.S. Azis, M.S. Mustaffa, A.H. Shaari, I. Ismail, H.C. Man, N.M. Saiden, N.H. Abdullah, Magnetite nanoparticles (MNPs) used as cadmium metal removal from the aqueous solution from mill scales waste sources, Sains Malays. 49 (2020) 847–858, https://doi.org/10.17576/jsm-2020-4904-14.

[120] G. Huang, J. Chen, S. Gao, Treatment of simulated steel pickling waste liquor by electrochemical synthesis of Fe3O4, water, Air. Soil Pollut. 231 (2020) 200237, https://doi.org/10.1007/s11270-020-04654-3.

[121] J. Tang, Y. Pei, Q. Hu, D. Pei, J. Xu, The recycling of ferric salt in steel pickling liquors: preparation of nano-sized iron oxide, Procedia Environ. Sci. 31 (2016) 778–784, https://doi.org/10.1016/j.proenv.2016.02.071.

[122] N.A.E. Emara, S.A. Elfeky, R.M. Amin, Antibacterial activity of magnetic nanoparticles synthesized from recycling of steel industry wastes antibacterial activity of magnetic nanoparticles synthesized from recycling of steel industry wastes view project strategic management view project nagy E, Int. J. Eng. Sci. Comput. 6 (2016) 8640. http://ijesc.org/.

[123] A. Blanco-Flores, H.P. Toledo-Jaldin, A.R. Vilchis-Néstor, G. López-Téllez, V. Sánchez-Mendieta, D.M. Ávila-Márquez, Metallurgical slag properties as a support material for bimetallic nanoparticles and their use in the removal of malachite green dye, Adv. Powder Technol. 31 (2020) 2853–2865, https://doi.org/10.1016/j.apt.2020.05.012.

[124] S. Salamat, H. Younesi, N. Bahramifar, Synthesis of magnetic core-shell Fe3O4@TiO2 nanoparticles from electric arc furnace dust for photocatalytic degradation of steel mill wastewater, RSC Adv. 7 (2017) 19391–19405, https://doi.org/10.1039/c7ra01238a.

[125] D.E. Rahmawati, L.M. Khoiroh, R. Ningsih, F. Yusniyanti, W. Solawati, P. Sari, Synthesis of hematite pigment (A- Fe2O3) from iron lathe waste using precipitation-sonication method as anti-swelling on wood, Int. J. Mech. Eng. Technol. Appl. (2020) 69–76.

[126] O. Karakas, E. Kanca, An investigation on optimum grinding system and conditions for steel plant ARP by-product α-Fe2O3 for pigment industry, Eng. Sci. Technol. an Int. J. 23 (2020) 1266–1272, https://doi.org/10.1016/j.jestch.2020.03.005.

[127] P. Kumaria, S. Kumara, A. Singhal, Magnetic Nanoparticle-Based Nanocontainers for Water Treatment, Elsevier Inc., 2019, https://doi.org/10.1016/B978-0-12-816770-0.00029-0.

[128] A. Kulpa-koterwa, T. Ossowski, P. Niedziałkowski, Functionalized Fe 3 O 4 nanoparticles as glassy carbon electrode modifiers for heavy metal ions detection — a mini review, Materials 14 (2021), https://doi.org/10.3390/ma14247725.

[129] L. Wang, X. Huang, C. Wang, X. Tian, X. Chang, Y. Ren, S. Yu, Applications of surface functionalized Fe3O4 NPs-based detection methods in food safety, Food Chem. 342 (2021) 128343, https://doi.org/10.1016/j.foodchem.2020.128343.

[130] A. Blanco-Flores, N. Arteaga-Larios, V. Pérez-García, J. Martínez-Gutiérrez, M. Ojeda-Escamilla, I. Rodríguez-Torres, Efficient fluoride removal using Al-Cu oxide nanoparticles supported on steel slag industrial waste solid, Environ. Sci. Pollut. Res. 25 (2018) 6414–6428, https://doi.org/10.1007/s11356-017-0849-6.

[131] S.F. Zhou, X.J. Han, Y.Q. Liu, SWASV performance toward heavy metal ions based on a high-activity and simple magnetic chitosan sensing nanomaterials, J. Alloys Compd. 684 (2016) 1–7, https://doi.org/10.1016/j.jallcom.2016.05.152.

[132] W. Wu, M. Jia, Z. Zhang, X. Chen, Q. Zhang, W. Zhang, P. Li, L. Chen, Sensitive, selective and simultaneous electrochemical detection of multiple heavy metals in environment and food using a lowcost Fe 3 O 4 nanoparticles/fluorinated multi-walled carbon nanotubes sensor, Ecotoxicol. Environ. Saf. 175 (2019) 243–250, https://doi.org/10.1016/j.ecoenv.2019.03.037.

[133] Z. Dahaghin, P.A. Kilmartin, H.Z. Mousavi, Novel ion imprinted polymer electrochemical sensor for the selective detection of lead(II), Food Chem. 303 (2020) 125374, https://doi.org/10.1016/j.foodchem.2019.125374.

[134] Z. Dahaghin, P.A. Kilmartin, H.Z. Mousavi, Simultaneous determination of lead(II) and cadmium(II) at a glassy carbon electrode modified with GO@Fe3O4@benzothiazole-2-carboxaldehyde using square wave anodic stripping voltammetry, J. Mol. Liq. 249 (2018) 1125–1132, https://doi.org/10.1016/j.molliq.2017.11.114.

[135] P. Wei, Z. Li, X. Zhao, R. Song, Z. Zhu, Fe3O4/SiO2/CS surface ion-imprinted polymer modified glassy carbon electrode for highly sensitivity and selectivity detection of toxic metal ions, J. Taiwan Inst. Chem. Eng. 113 (2020) 107–113, https://doi.org/10.1016/j.jtice.2020.08.035.

[136] B. Fall, A.K.D. Diaw, M. Fall, M.L. Sall, M. Lo, D. Gningue-sall, M. Ottakam, H.J. Maria, N. Kalarikkal, S. Thomas, Synthesis of highly sensitive rGO @ CNT @ Fe 2 O 3/polypyrrole nanocomposite for the electrochemical detection of Pb 2 +, Mater. Today Commun. 26 (2021) 102005 https://doi.org/10.1016/j.mtcomm.2020.102005.

[137] M. Simsek, N. Wongkaew, Carbon nanomaterial hybrids via laser writing for high-performance non-enzymatic electrochemical sensors: a critical review, Anal. Bioanal. Chem. 413 (2021) 6079–6099, https://doi.org/10.1007/s00216-021-03382-9.

[138] E.M. Bakhsh, S. Bahadar, A.M. Asiri, A. Shah, Zn/Fe nanocomposite based efficient electrochemical sensor for the simultaneous detection of metal ions, Phys. E Low-Dimensional Syst. Nanostructures. 130 (2021) 114671, https://doi.org/10.1016/j.physe.2021.114671.

[139] S. Li, W. Zhou, M. Jiang, L. Li, Y. Sun, Z. Guo, X. Huang, M. Jiang, Z. Guo, Insights into diverse performance for the electroanalysis of Pb(II) on Fe2O3 nanorods and hollow nanocubes: toward analysis of adsorption sites, Electrochim. Acta (2018), https://doi.org/10.1016/j.electacta.2018.08.069.

[140] J. Liao, Z. Tao, S. Lin, Theoretical and experimental insights into the electrochemical heavy metal ion sensing with nonconductive nanomaterials, Curr. Opin. Electrochem. 17 (2019) 1–6, https://doi.org/10.1016/j.coelec.2019.04.006.

[141] G. Ziyatdinova, L. Gimadutdinova, Cerium(IV) and iron(III) oxides nanoparticles based voltammetric sensor for the sensitive and selective determination of lipoic acid, Sensors 21 (2021), https://doi.org/10.3390/s21227639.
[142] V. Izadkhah, M. Rezaei, J. Mahmoodi, A new platform based on the Fe 3 O 4 nanoparticles, ligand and ionic liquid: application to the sensitive electrochemical determination of the lead ion in water and fish samples, Anal. Bioanal. Chem. Res. 6 (2019) 405–417.
[143] A. Khoobi, N. Soltani, M. Aghaei, Computational design and multivariate statistical analysis for electrochemical sensing platform of iron oxide nanoparticles in sensitive detection of anti-inflammatory drug diclofenac in biological fluids, J. Alloys Compd. 831 (2020) 154715, https://doi.org/10.1016/j.jallcom.2020.154715.
[144] K. Amanda, R. Jacek, G. Skowierzak, A. Koterwa, G. Schroeder, T. Ossowski, P. Niedziałkowski, Comparison of cadmium Cd2+ and lead Pb2+ binding by Fe2O3@SiO2-EDTA nanoparticles – binding stability and kinetic studies, Electroanalysis 32 (2020) 588–597, https://doi.org/10.1002/elan.201900616.
[145] M. Afzali, A. Mostafavi, Z. Afzali, T. Shamspur, Designing a rapid and selective electrochemical nanosensor based on molecularly imprinted polymer on the Fe3O4/MoS2/glassy carbon electrode for detection of immunomodulatory drug pomalidomide, Microchem. J. 164 (2021) 106039, https://doi.org/10.1016/j.microc.2021.106039.
[146] O.E. Fayemi, A.S. Adekunle, B.E. Kumara Swamy, E.E. Ebenso, Electrochemical sensor for the detection of dopamine in real samples using polyaniline/NiO, ZnO, and Fe3O4 nanocomposites on glassy carbon electrode, J. Electroanal. Chem. 818 (2018) 236–249, https://doi.org/10.1016/j.jelechem.2018.02.027.
[147] R. Srivastava, Synthesis and characterization techniques of nanomaterials, Int. J. Green Nanotechnol. 4 (2012) 17–27, https://doi.org/10.1080/19430892.2012.654738.
[148] F. Bahador, R. Foroutan, H. Esmaeili, B. Ramavandi, Enhancement of the chromium removal behavior of Moringa oleifera activated carbon by chitosan and iron oxide nanoparticles from water, Carbohydr. Polym. 251 (2021) 117085, https://doi.org/10.1016/j.carbpol.2020.117085.
[149] A. Šutka, S. Lagzdina, T. Käämbre, R. Pärna, V. Kisand, J. Kleperis, M. Maiorov, A. Kikas, I. Kuusik, D. Jakovlevs, Study of the structural phase transformation of iron oxide nanoparticles from an Fe2+ ion source by precipitation under various synthesis parameters and temperatures, Mater. Chem. Phys. 149 (2015) 473–479, https://doi.org/10.1016/j.matchemphys.2014.10.048.
[150] W. Boumya, N. Taoufik, M. Achak, N. Barka, Chemically modified carbon-based electrodes for the determination of paracetamol in drugs and biological samples, J. Pharm. Anal. 11 (2021) 138–154, https://doi.org/10.1016/j.jpha.2020.11.003.
[151] N.T.A. Thu, H. Van Duc, N. Hai Phong, N.D. Cuong, N.T.V. Hoan, D. Quang Khieu, Electrochemical determination of paracetamol using Fe3O4/reduced graphene-oxide-based electrode, J. Nanomater. 2018 (2018), https://doi.org/10.1155/2018/7619419.
[152] D. Gounden, S. Khene, N. Nombona, Electroanalytical detection of heavy metals using metallophthalocyanine and silica - coated iron oxide composites, Chem. Pap. (2018), https://doi.org/10.1007/s11696-018-0545-0.
[153] G. Bharath, R. Madhu, S.M. Chen, V. Veeramani, D. Mangalaraj, N. Ponpandian, Solvent-free mechanochemical synthesis of graphene oxide and Fe3O4-reduced graphene oxide nanocomposites for sensitive detection of nitrite, J. Mater. Chem. A 3 (2015) 15529–15539, https://doi.org/10.1039/c5ta03179f.
[154] M.N. Nor, S. Arivalakan, N.D. Zakaria, N. Nilamani, Z. Lockman, K. Abdul Razak, Self-Assembled iron oxide nanoparticle-modified APTES-ITO electrode for simultaneous stripping analysis of Cd(II) and Pb(II) ions, ACS Omega 7 (2022) 3823–3833, https://doi.org/10.1021/acsomega.1c07158.
[155] M. Mazloum-Ardakani, M. Maleki, A. Khoshroo, High-performance electrochemical sensor based on electrodeposited iron oxide nanoparticle: catecholamine as analytical probe, J. Iran. Chem. Soc. 14 (2017) 1659–1664, https://doi.org/10.1007/s13738-017-1106-0.
[156] Y.C. Eeu, H.N. Lim, Y.S. Lim, S.A. Zakarya, N.M. Huang, Electrodeposition of polypyrrole/reduced graphene oxide/iron oxide nanocomposite as supercapacitor electrode material, J. Nanomater. 2013 (2013), https://doi.org/10.1155/2013/653890.
[157] S. Saha, J.S. Kumar, N. Chandra Murmu, P. Samanta, T. Kuila, Controlled electrodeposition of iron oxide/nickel oxide@Ni for the investigation of the effects of stoichiometry and particle size on energy storage and water splitting applications, J. Mater. Chem. A 6 (2018) 9657–9664, https://doi.org/10.1039/c8ta00795k.
[158] D. Manoj, S. Shanmugasundaram, C. Anandharamakrishnan, Nanosensing and nanobiosensing: concepts, methods, and applications for quality evaluation of liquid foods, Food Control 126 (2021), https://doi.org/10.1016/j.foodcont.2021.108017.
[159] M. Elrouby, N. Abo El-Maali, R. Abd El-Rahman, A promising electrodeposited iron oxide nanoparticles of very high saturation magnetization and superparamagnetic properties for remediation of polluted water with lead ions, J. Taiwan Inst. Chem. Eng. 93 (2018) 379–387, https://doi.org/10.1016/j.jtice.2018.08.004.
[160] P. Jakubec, V. Urbanová, Z. Medříková, R. Zbořil, Advanced sensing of antibiotics with magnetic gold nanocomposite: electrochemical detection of chloramphenicol, Chem. Eur J. 22 (2016) 14279–14284, https://doi.org/10.1002/chem.201602434.
[161] S. Xiong, B. Yang, D. Cai, G. Qiu, Z. Wu, Individual and simultaneous stripping voltammetric and mutual interference analysis of Cd2+, Pb2+ and Hg2+ with reduced graphene oxide-Fe3O4 nanocomposites, Electrochim. Acta 185 (2015) 52–61, https://doi.org/10.1016/j.electacta.2015.10.114.
[162] K. Thangavelu, J.A. Allen, S.-M. Chen, C. Viswanathan, K. Krishna, Trace level electrochemical determination of neurotransmitter dopamine in biological samples based on iron oxide nanoparticles decorated graphene sheets, Inorg. Chem. Front. (2018), https://doi.org/10.1039/C7QI00716G.
[163] H. Hu, W. Lu, X. Liu, F. Meng, J. Zhu, A high-response electrochemical as (III) sensor using Fe3O 4 – rGO nanocomposite materials, Chemosensors 9 (2021), https://doi.org/10.3390/chemosensors9060150.
[164] Y. Haowei, H. Shuangqi, Electrochemical sensing of heavy metal ions based on monodisperse single-crystal Fe 3 O 4 microspheres, J. Wuhan Univ. Technol. Sci. 33 (2018) 1422–1427, https://doi.org/10.1007/s11595-018-1985-7.
[165] Z. Nate, A.A.S. Gill, S. Shinde, R. Chauhan, S.N. Inamdar, R. Karpoormath, A simple in-situ flame synthesis of nanocomposite (MWCNTs-Fe2O3) for electrochemical sensing of proguanil in pharmaceutical formulation, Diam. Relat. Mater. 111 (2021) 108178, https://doi.org/10.1016/j.diamond.2020.108178.
[166] Z. Xu, X. Fan, Q. Ma, B. Tang, Z. Lu, J. Zhang, G. Mo, J. Ye, J. Ye, A sensitive electrochemical sensor for simultaneous voltammetric sensing of cadmium and lead based on Fe3O4/multiwalled carbon nanotube/laser scribed graphene composites functionalized with chitosan modified electrode, Mater. Chem. Phys. 238 (2019) 121877, https://doi.org/10.1016/j.matchemphys.2019.121877.
[167] R.D. Nagarajan, A. Sundaramurthy, A.K. Sundramoorthy, Synthesis and characterization of MXene (Ti3C2Tx)/Iron oxide composite for ultrasensitive electrochemical detection of hydrogen peroxide, Chemosphere 286 (2022), https://doi.org/10.1016/j.chemosphere.2021.131478.
[168] S. Lameche, S.E. Berrabah, A. Benchettara, S. Tabti, A. Manseri, D. Djadi, J.F. Bardeau, One-step electrochemical elaboration of SnO2 modified electrode for lead ion trace detection in drinking water using SWASV, Environ. Sci. Pollut. Res. 30 (2023) 44578–44590, https://doi.org/10.1007/s11356-023-25517-4.
[169] L. Wang, T. Lei, Z. Ren, X. Jiang, X. Yang, H. Bai, S. Wang, Fe 3 O 4 @ PDA @ MnO 2 core-shell nanocomposites for sensitive electrochemical detection of trace Pb (II) in water, J. Electroanal. Chem. 864 (2020) 114065, https://doi.org/10.1016/j.jelechem.2020.114065.
[170] S. Mohammadi, M.A. Taher, H. Beitollahi, Synthesis and application of a natural-based nanocomposite with carbon nanotubes for sensitive voltammetric determination of lead (II) ions, Int. J. Environ. Anal. Chem. 100 (2020) 65–81, https://doi.org/10.1080/03067319.2019.1631300.
[171] C. Guo, C. Wang, H. Sun, D. Dai, H. Gao, A simple electrochemical sensor based on rGO/MoS2/CS modified GCE for highly sensitive detection of Pb(ii) in tobacco leaves, RSC Adv. 11 (2021) 29590–29597, https://doi.org/10.1039/d1ra05350g.
[172] M.S. Tamwa, J.R. Njimou, B.B. Nguelo, C.P. Nanseu-Njiki, E. Vunain, B.C. Tripathy, E. Ngameni, Electrochemical sensor based on green-synthesized iron oxide nanomaterial modified carbon paste electrode for Congo red electroanalysis and capacitance performance, Mater. Res. Innovat. 27 (2023) 243–252, https://doi.org/10.1080/14328917.2022.2125694.
[173] M. Baghayeri, H. Alinezhad, M. Fayazi, M. Tarahomi, R. Ghanei-Motlagh, B. Maleki, A Novel Electrochemical Sensor Based on a Glassy Carbon Electrode Modified with Dendrimer Functionalized Magnetic Graphene Oxide for Simultaneous Determination of Trace Pb(II)and Cd(II), Elsevier Ltd, 2019, https://doi.org/10.1016/j.electacta.2019.04.180.
[174] G. Li, X. Qi, Y. Xiao, Y. Zhao, K. Li, Y. Xia, X. Wan, J. Wu, C. Yang, An efficient voltammetric sensor based on graphene oxide-decorated binary transition metal oxides Bi2O3/MnO2 for trace determination of lead ions, Nanomaterials 12 (2022), https://doi.org/10.3390/nano12193317.
[175] M. Bagherzadeh, M. Pirmoradian, F. Riahi, Electrochemical detection of Pb and Cu by using DTPA functionalized magnetic nanoparticles, Electrochim. Acta 115 (2014) 573–580, https://doi.org/10.1016/j.electacta.2013.11.012.

[176] U.O. Aiigbe, R.B. Onyancha, K.E. Ukhurebor, O.A. Osibote, M.A. Onoyivwe, H.I. Atagana, P.O. Ogbemudia, S.P. Akanji, Electrochemical detection of heavy metals, in: M.A. Onoyivwe, S.R. Suprakas, P.O. Osifo (Eds.), Modif. Nanomater. Environ. Appl., Springer, Cham, 2022, pp. 25–63, https://doi.org/10.1007/978-3-030-85555-0.
[177] Y. Beyene, Z. Bitew, F. Fekade, Electrochemical detection of Pb(ii) and Cd(ii) using bismuth ferrite nanoparticle modified carbon paste electrodes, Mater. Adv. 3 (2022) 5882–5892, https://doi.org/10.1039/d2ma00133k.
[178] A. Mourya, S.K. Sinha, B. Mazumdar, Glassy carbon electrode modified with blast furnace slag for electrochemical investigation of Cu 2+ and Pb 2+ metal ions, Microchem. J. 147 (2019) 707–716, https://doi.org/10.1016/j.microc.2019.03.082.
[179] O.R. Obisesan, A.S. Adekunle, J.A.O. Oyekunle, T. Sabu, T.T.I. Nkambule, B.B. Mamba, Development of electrochemical nanosensor for the detection of malaria parasite in clinical samples, Front. Chem. 7 (2019) 1–15, https://doi.org/10.3389/fchem.2019.00089.
[180] K.P. Gannavarapu, V. Ganesh, R.B. Dandamudi, Zirconia nanocomposites with carbon and iron(iii) oxide for voltammetric detection of sub-nanomolar levels of methyl parathion, Nanoscale Adv. 1 (2019) 4947–4954, https://doi.org/10.1039/c9na00589g.
[181] A.S. Adekunle, S. Lebogang, P.L. Gwala, T.P. Tsele, L.O. Olasunkanmi, O.E. Fayemi, B. Diseko, N. Mphuthi, J.A.O. Oyekunle, A.O. Ogunfowokan, E.E. Ebenso, Electrochemical response of nitrite and nitric oxide on graphene oxide nanoparticles doped with, RSC Adv. 5 (2015) 27759–27774, https://doi.org/10.1039/C5RA02008E.
[182] H.A. Hamid, Z. Lockman, N.M. Nor, N.D. Zakaria, K.A. Razak, Sensitive detection of Pb ions by square wave anodic stripping voltammetry by using iron oxide nanoparticles decorated zinc oxide nanorods modified electrode, Mater. Chem. Phys. 273 (2021) 125148, https://doi.org/10.1016/j.matchemphys.2021.125148.
[183] L. Xiao, B. Wang, L. Ji, F. Wang, Q. Yuan, G. Hu, A. Dong, W. Gan, An efficient electrochemical sensor based on three-dimensionally interconnected mesoporous graphene framework for simultaneous determination of Cd(II) and Pb(II), Electrochim. Acta 222 (2016) 1371–1377, https://doi.org/10.1016/j.electacta.2016.11.113.
[184] D. Shahnaz, M.H. Givianrad, M. Saber-Tehrani, P.A. Azar, Electrochemical sensing system based on MnFe2O4/rGO for simultaneous determination of trace amount Pb2+ and Cd2+ in spice samples, Russ. J. Electrochem. 56 (2020) 506–517, https://doi.org/10.1134/S1023193520060051.
[185] S. Benabid, A.F.M. Streit, Y. Benguerba, G.L. Dotto, A. Erto, B. Ernst, Molecular modeling of anionic and cationic dyes adsorption on sludge derived activated carbon, J. Mol. Liq. 289 (2019) 111119, https://doi.org/10.1016/j.molliq.2019.111119.
[186] B. Hu, Z. Gao, H. Wang, J. Wang, M. Cheng, Computational insights into the sorption mechanism of polycyclic aromatic hydrocarbons by carbon nanotube through density functional theory calculation and molecular dynamics simulation, Comput. Mater. Sci. 179 (2020) 109677, https://doi.org/10.1016/j.commatsci.2020.109677.
[187] H.A. Mashhadzadeh, A.M. Ghorbanzadeh, A. Salmankhani, M. Fataliyan, Density functional theory study of adsorption properties of non-carbon, carbon and functionalized graphene surfaces towards the zinc and lead atoms, Phys. E Low-Dimensional Syst. Nanostructures. 104 (2018) 275–285, https://doi.org/10.1016/j.physe.2018.08.010.
[188] M. Liu, L. Zhu, X. Zhang, W. Han, Y. Qiu, Insight into the role of ion-pairing in the adsorption of imidazolium derivative-based ionic liquids by activated carbon, Sci. Total Environ. 743 (2020) 140644, https://doi.org/10.1016/j.scitotenv.2020.140644.
[189] B. Huang, X. Luo, Q. Pu, J. Guo, X. Tong, X. Lu, Simultaneous detection of Pb 2+ and Cu 2+ on β-CD-NH2 -Fe3O4 modified electrode, ChemistrySelect 7 (2022), https://doi.org/10.1002/slct.202104443.